Fluid transients in viscoelastic pipes via an internal variable constitutive theory

Applied Mathematical Modelling 114 (2023) 846–869

Contents lists available at ScienceDirect

Applied Mathematical Modelling

journal homepage: www.elsevier.com/locate/apm

Fluid transients in viscoelastic pipes via an internal variable constitutive theory

Douglas Monteiro Andrade [a,*], Felipe Bastos de Freitas Rachid [a], Arris Sieno Tijsseling [b]

[a] Graduate Program in Mechanical Engineering (PGMEC), Department of Mechanical Engineering (TEM), Universidade Federal Fluminense, Rua Passo da Pátria, 156, 24210-240, Niterói, RJ, Brazil
[b] Dept. of Mathematics and Computer Science, Eindhoven University of Technology, P.O. Box 513, 5600 MB Eindhoven, the Netherlands

ARTICLE INFO

Article history:
Received 4 July 2022
Revised 27 September 2022
Accepted 17 October 2022
Available online 21 October 2022

Keywords:
Unsteady flow
Fluid transient
Viscoelastic pipe
Internal variables
Energy dissipation

ABSTRACT

This work presents a fluid transient model capable of handling the viscoelastic behavior of the pipe. A previously developed quasi-2D flow model is employed as a base, and the viscoelastic behavior of the pipe is incorporated by considering constitutive equations formulated in a thermodynamically consistent framework of an internal variable theory. Such an approach straightforwardly provides expressions for computing the rates of energy dissipation in the fluid and pipe accurately and separately. This novel feature discerns the local and overall impacts of the energy dissipation on the pressure oscillations caused by each medium. The governing equations of the model form a hyperbolic system of partial differential equations whose approximated solutions are obtained by the method of characteristics. Taking as reference pressure signals obtained by a classic reservoir-pipe-valve experiment found in the literature, it is shown that the model predictions are fully consistent. A comparison between the pressure responses of viscoelastic and elastic pipes reveals that in addition to delaying the pressure oscillations, the viscoelastic behavior causes a faster attenuation of them. The rates of energy dissipation in the viscoelastic pipe attain significant magnitudes during the first moments of the fluid transient and alters the hydrodynamical behavior of the flow. Such interference is exposed by comparing the responses of the same experimental setup when two different viscoelastic pipe materials are considered. It is also shown that the knowledge of the parcels of energy dissipated in the fluid and pipe individually can improve the comprehension of the phenomenon and be utilized for theoretical and applied research in the field.

1. Introduction

Transient flows in pipeline systems are intrinsic phenomena in any operational piping system. Both abnormal and normal circumstances can lead to flow unsteadiness, such as mandatory valve maneuvers or unpredicted pump failures. The dynamics of such flows are governed by a cyclic passage of waves in the fluid which are responsible for local pressure surges. These pressure traces subject the compliant pipe to higher stresses than those found under a steady-state regime.

* Corresponding author.
E-mail addresses: dmajnj@gmail.com (D.M. Andrade), frachid@id.uff.br (F.B. de Freitas Rachid), a.s.tijsseling@tue.nl (A.S. Tijsseling).

https://doi.org/10.1016/j.apm.2022.10.024
0307-904X/

As those fluctuations depend not only on the fluid and the nature of the flow but also on the mechanical response of the material of which the tubes are made, a proper analysis of this phenomenon requires the description of all these aspects.

In the industrial context, depending on the type of application, tubes of different materials are used, giving rise to different mechanical responses. Typical industrial pipe systems are made with steels of different carbon contents, which exhibit linear elastic behavior in the scope of applications. On the other hand, sanitary sewer and water supply pipes are usually made of polymeric materials like polyvinyl chloride (PVC), polybutylene (PB), low-density polyethylene (LDPE), and high-density polyethylene (HDPE), which respond to hydraulic loading with a viscoelastic mechanical response [1–3]. In the last decades, the application of these materials in a diverse range of industrial applications has increased due to their attractive mechanical and chemical properties aside from their lower costs [4]. However, although their properties are well-suited to many in-practice usages, the traditional quasi-one-dimensional fluid transient theory [5], which assumes elastic behavior of the pipeline, is not suited to accurately describe the behavior of the fluid-pipe system [6]. The pipe material's viscoelasticity significantly alters the system's responses by adding dispersive and dissipative effects to pressure waves propagating in the liquid [1].

Due to the uprising use of this kind of materials, research has been undertaken to model properly the fluid transients in viscoelastic pipes thereby following two different approaches. In one of them, researchers incorporated the viscoelastic behavior of the pipe into the classic fluid transient theory by assuming that the viscoelasticity turns the wavefront into a frequency-dependent phenomenon [7]. On the other, the wavefront propagation is treated as constant, as a result of assuming that the volumetric deformation of the pipe material is purely elastic, whereas the deformation associated with shear presents both elastic and viscoelastic responses [8]. The latter was achieved by considering that the strains and their evolution are described with generalized Kelvin-Voigt elements and hereditary integrals (convolutions). After this first essential step, other effects that notably impact the transient responses, ignored by these pioneering works, were included in more recent modeling works.

Güney [9] made a great contribution to the field when he conceived a model which incorporated the quasi-one-dimensional (quasi-1D) unsteady-friction model for laminar flows developed by Zielke [10] into the context of Gally's viscoelastic model. Covas et al. [11] expanded his work by employing quasi-1D unsteady friction models for both laminar and turbulent flows into the same (Gally's) framework. Even though the quasi-1D modeling is useful to predict pressure surges, it cannot conceive velocity profiles of the flow, which are essential to the thermomechanical description of the transient flow [12–13]. Pezzinga et al. [14] and Wahba [15] developed quasi-2D models in viscoelastic pipes to better comprehend the phenomenon. The former claims that the decay of the pressure oscillations is closely related to the phase shift between the pressure signals and the anelastic circumferential strains. Numerical simulations also show that velocity profiles in viscoelastic pipes are flatter than those found in elastic pipes. On the other hand, the latter focused on a parametric study of unsteady laminar flows in viscoelastic pipes to demonstrate the impact of two dimensionless parameters on transient responses. Several other features have been explored in the past decade, such as the presence of in-line valves or sudden cross-section changes [16–17] and pipe networks [18–19]. Soares et al. [20], Urbanowicz et al. [21], and Mousavifard [22] also studied the effects of cavitating flows in viscoelastic pipes. Meanwhile, other works were concerned with identifying pipe faults/anomalies in viscoelastic pipelines, as broadly presented by Che et al. [23].

The energy transfer and dissipation evolution in fluid transients are crucial to the proper design of piping systems as it provides sound tools for the analysis of the local and overall behavior of the fluid-pipe system [24]. In the case of the applications involving viscoelastic pipes, the dissipative nature of these materials influences the energy transfer and redistribution throughout these piping systems. Indeed, researchers have focused on the application of viscoelastic pipes as energy dissipators to reduce overpressure in piping systems [25–32]. Despite the foremost role of energy analysis, to the best of the authors' knowledge, few works have been dedicated to these energy-related issues of fluid transients in viscoelastic pipes. Duan et al. [12] studied the bidirectional energy transfer between the pipe and fluid by applying the energy relations derived by Karney [33]. Pan et al. [34] extended this analysis by presenting the energy transmission diagrams that expose the importance of dissipative phenomena such as steady friction, unsteady friction, and pipe viscoelasticity for an extensive range of transient intensities and frequencies of excitations.

Aiming to advance a step forward, the present work proposes a new perspective to energy analysis by presenting a mechanical formulation of fluid transients that accurately and straightforwardly determine the energy dissipation in both viscoelastic pipe and fluid. The present model takes advantage of a quasi-2D fluid-transient model that has been validated recently, along with a consolidated viscoelastic model developed in the framework of the thermodynamics of irreversible processes with internal variables [35–36]. As a result, expressions for the computation of the rates of energy dissipation in the fluid and pipe are straightforwardly derived. As both fluid and pipe models are thermodynamically consistent, the proposed approach can account for isolated and accurate estimates of energy dissipation rates in the fluid and the tube. This novel feature can not only be fruitful to enhance the theoretical knowledge about this phenomenon as demonstrated herein, but also provide a promising tool for energy-based design techniques of pipeline systems.

The proposed model and approach are validated by comparing their numerical predictions against experimental data found in the literature. By appealing to a comparison between the proposed model predictions with and without pipe viscoelasticity, the present work shows that faster attenuation and delayed responses of the pressure oscillations are found in the viscoelastic case. Access to the rates of energy dissipation in the fluid and pipe sheds light on the central thermomechanical effect behind those different results: the significant levels of energy dissipated in the pipe due to the viscoelasticity. In the course of this analysis, the pipe and fluid mechanical coupling is constantly investigated. Such coupling is ultimately

exposed when the model responses for the same fluid flow installations with two different viscoelastic pipe materials are inspected.

2. Basic equations

The basic equations that describe an unsteady flow inside a deformable circular pipe can be achieved by using the quasi-2D model developed by Andrade and Freitas Rachid [37]. This model has used the framework of the theory of mixtures [38] to describe the fluid as a pseudo-mixture formed by a set of n shell-shaped constituents. They are assumed to hold the same fluid properties and be concentrically distributed in the radial direction, r, of the pipe. In this context, these constituents act like fluid layers having their own motion along the direction of the pipe center-line with speeds $v_j\{j = 1, \ldots, n\}$. Each one of these j-indexed constituents is characterized by its thickness ΔR_j, central radius $R_j = R_{j-1} + \Delta R_{j-1}/2 + \Delta R_j/2$, with $R_0 \equiv 0 \equiv \Delta R_0$, and fixed area fraction $\alpha_j = 2R_j\Delta R_j/R^2$, such that $\sum_{j=1}^{n}\alpha_j = 1$ and $\sum_{j=1}^{n}\Delta R_j = R$, where R is the undisturbed internal radius of the pipe. In addition, the mass density and pressure of the pseudo-mixture as a whole are defined as $\rho = \sum_{j=1}^{n}\rho_j$ and $p = \sum_{j=1}^{n}p_j$, respectively, in which $\rho_j = \alpha_j\rho$ and $p_j = \alpha_j p$ stand for these variables in the $j-th$ constituent. Meanwhile, the mean velocity of the pseudo-mixture is conceived to obey the requirement that the total mass flow rate per unit volume is the sum of the individual mass flow rates of the constituents, so that $v = \sum_{j=1}^{n}\rho_j v_j/\sum_{j=1}^{n}\rho_j = \sum_{j=1}^{n}\alpha_j v_j$, in which v_j is the mean velocity in each $j-th$ constituent. Fig. 1 is a sketch of the pseudo-mixture structure proposed for the fluid flow.

By assuming that the fluid is Newtonian and slightly compressible and that the pipe has negligible inertia and is subjected to small deformation and axisymmetric plane-stress distribution, the mechanical balance laws of the proposed model can be expressed as:

$$\frac{1}{K}\frac{\partial p}{\partial t} + \rho_0\frac{\partial v}{\partial x} + 2\frac{\partial \varepsilon_\theta|_{r=R}}{\partial t} = 0, \tag{1}$$

$$\rho_0\frac{\partial v}{\partial t} + \frac{\partial p}{\partial x} + \frac{2}{R}\sum_{j=1}^{n}a_j = 0, \tag{2}$$

$$\alpha_j\rho_0\frac{\partial v_j}{\partial t} + \alpha_j\frac{\partial p}{\partial x} + m_j + \frac{2}{R}a_j = 0,\ j = 2, \ldots, n, \tag{3}$$

where ε_θ, K and ρ_0 are the principal circumferential strain of the pipe, fluid bulk modulus and the undisturbed fluid density, respectively. Further, a_j represents the skin friction force per unit of cylindrical area that acts on the fluid-pipe interface, and m_j represents the axial internal interaction force per unit of volume exerted by the other constituents on the $j-th$ constituent [37]. These equations represent the mass and momentum balances for the mixture as a whole, and the balance of momentum for each $j-th$ constituent except for the first, respectively. Only $n-1$ balances of momentum for constituents are required since the present modeling includes the mixture velocity v, which is a linear combination of the independent velocities of each constituent v_j, as a dependent variable.

To complete the modeling, constitutive equations that describe the interaction forces acting on the pseudo-mixture and proper pipe stress-strain relations for a viscoelastic pipe are needed.

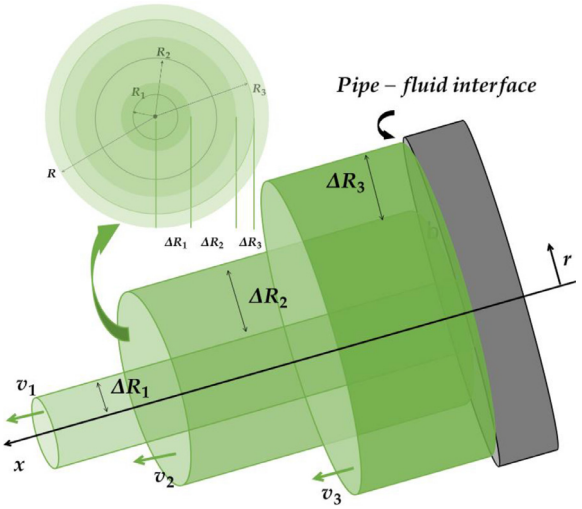

Fig. 1. Virtual structure of the pseudo-mixture for $n = 3$.

3. CONSTITUTIVE EQUATIONS

3.1. Fluid constitutive equations

The constitutive equations of the "forces" m_j and a_j are addressed by appealing to the material frame indifference principle and the aforementioned kinematic aspects of the structured mixture. The proposed forms for m_j and a_j are given by:

$$m_j = C_{j,j-1}\left(v_j - v_{j-1}\right) + C_{j,j+1}\left(v_j - v_{j+1}\right) \text{ for } j = 1, \ldots, \ n, \text{ with } C_{1,0} \equiv 0 \text{ and } C_{n,n+1} \equiv 0 \tag{4}$$

$$a_j = \begin{cases} 0, \ j = 1, \ldots., \ n-1 \\ Cv_n, \ j = n \end{cases}, \tag{5}$$

in which C_{jj-1}, C, and $C_{j,j+1}$ are material constants of the model. By appealing to the action-reaction principle, we observe that $C_{jj+1} = C_{j+1,j}$ such that C, $C_{j,j+1}$ are sufficient to completely describe the constitutive equations of the pseudo-mixture given by Eqs. (4-5). These material constants can be found through the assumption that during the transient regime the viscosity structure remains the same as in the permanent regime (i.e., frozen viscosity, see Vardy et al. [39]). Thus, the steady-state momentum balances for the $j-th$ constituents Eq. 3), along with Eqs. (4-(5) and a given fully-developed velocity profile in a flow of an incompressible fluid can be employed to generate a linear system of equations given by

$$\alpha_j \frac{\partial p}{\partial x} + m_j + \frac{2}{R} a_j = 0, \ j = 1, \ldots, \ n, \tag{6}$$

whose solution gives the material constants C and $C_{j,j+1}$ of the model. This approach is general and therefore holds for both laminar and turbulent flows; it is exposed in detail in Appendix A. Applying the classic parabolic-shape laminar velocity profile in Eq. (6), the following material constants of the model result:

$$C_{j,j+1} = \frac{4\rho_0 \nu}{R_{j+1}^2 - R_j^2}\left(\sum_{i=1}^{j} \alpha_i\right), \text{ with } R_{n+1} \equiv 0 \tag{7}$$

$$C = \frac{2\ \rho_0 \nu R}{R^2 - R_n^2}, \tag{8}$$

in which ν is the fluid's kinematic viscosity.

For turbulent flows, the algebraic turbulence model described by Vardy and Brown [40] is applied to obtain an expression for the velocity profile. This approach adopts an idealized turbulence viscosity distribution with two distinct regions: an outer annulus and an inner core. The core region ranges from $r = 0$ to $r = R_M = 0.8R$ and has a fixed turbulence kinematic viscosity ν_c while in the annulus, with a thickness equal to $b = 0.2\,R$, the turbulent kinematic viscosity varies linearly from the value ν_w at the wall $r = R$, to the value ν_c at the interface of these regions. As the turbulence model has a piecewise distribution, in addition to the classical non-slip condition at the wall and axial symmetry of the flow, interface boundary conditions must be stated. Within this framework, the velocity profile found is given by [37]

$$v(r) = \begin{cases} \dfrac{\left(-\frac{dp}{dx}\right)}{\rho_0 \nu_w}\left\{\dfrac{\left(R_M^2 - r^2\right)}{4(\sigma_{cw})} - \dfrac{b^2}{2}\left[\dfrac{-1}{(1-\sigma_{cw})} + \dfrac{(-4+5\sigma_{cw})}{(1-\sigma_{cw})^2}\ln\left(\dfrac{1}{\sigma_{cw}}\right)\right]\right\}, \ 0 \le r \le R_M \\ \dfrac{\left(-\frac{dp}{dx}\right)}{2\nu_w\ \rho_0}\dfrac{b^2}{}\left\{\dfrac{(R-r)}{(1-\sigma_{cw})b} + \dfrac{(4-5\sigma_{cw})}{(1-\sigma_{cw})^2}\ln\left[\dfrac{1}{\frac{(1-\sigma_{cw})}{b}r\ -4+5\sigma_{cw}}\right]\right\}, \ R_M < r \le R \end{cases}, \tag{9}$$

where $\sigma_{cw} = \nu_c/\nu_w$ is the ratio of the kinematic eddy viscosities. From this velocity profile, the material constants associated with the interaction forces in the core and annulus regions are:

$$C_{j,j+1} = \frac{4\rho_0 \nu_c}{R_{j+1}^2 - R_j^2}\left(\sum_{i=1}^{j} \alpha_i\right), \tag{10}$$

$$C_{j,j+1} = \frac{2\nu_w \rho_0 (1-\sigma_{cw})/b^2}{\left\{\frac{R_{j+1}-R_j}{b} + \frac{(-4+5\sigma_{cw})}{(1-\sigma_{cw})}\ln\left[\frac{\left(\frac{1-\sigma_{cw}}{b}\right)R_j - 4 + 5\sigma_{cw}}{\left(\frac{1-\sigma_{cw}}{b}\right)R_{j+1} - 4 + 5\sigma_{cw}}\right]\right\}}\left(\sum_{i=1}^{j} \alpha_i\right), \text{ with } R_{n+1} \equiv 0, \tag{11}$$

respectively whereas that related to the skin friction material constant can be expressed as:

$$C = \frac{\nu_w \rho_0 R(1-\sigma_{cw})/b^2}{\left\{\frac{R-R_n}{b} + \frac{(-4+5\sigma_{cw})}{(1-\sigma_{cw})}\ln\left[\left(\frac{1-\sigma_{cw}}{b}\right)R_n\ -4+5\sigma_{cw}\right]\right\}}. \tag{12}$$

The material constants given by Eqs. (7-8) and Eqs. (10-12) play a crucial role in the radial momentum diffusion through the discrete fluid layers. This becomes clear when the shear stress acting on each of these constituents is invoked:

$$\tau_j = \begin{cases} \frac{R_j}{2}\left[C_{j,j+1}\left(v_j - v_{j+1}\right)\right], & for \;\; j = 1,\; n-1, \\ a_n, & for \;\; j = n. \end{cases} \tag{13}$$

By looking at Eq. (13), and summing up all equations in Eq. (6), it results in $a_n \equiv Cv_n = -\frac{R}{2}\frac{\partial p}{\partial x}$. Thus, the skin friction force a_n acts just like the wall shear stress τ_w in the present model, as expected and validating the method.

3.2. Pipe constitutive equations

This work adopts the consolidated thermodynamics of irreversible processes with internal variables [35–36] to describe the viscoelastic mechanical behavior of the pipe. Essentially, this theory relies on the assumption that the thermodynamic state of a material medium, at any point and instant, is characterized by a set of observable and internal state variables. In the present application, internal variables are introduced to describe the material's anelasticity and its associated dissipative phenomena. Within this framework, two thermodynamic potentials are employed to derive the constitutive equations: the Helmholtz free energy potential and a pseudo-potential of dissipation. The first potential describes the reversible relationship between state variables and associated thermodynamic forces, from which state laws are obtained. The second portrays the irreversible character of the material associated with dissipative phenomena, from which evolution laws are postulated. These state and evolution laws form the set of constitutive equations of the material.

The selection of the internal variables is a constitutive choice and depends on the desired degree of detail of the material's internal structure therefore it can vary from problem to problem. The role of these variables will become clearer ahead when a particular family of constitutive equations for a specific viscoelastic material is presented. In the meantime, the constitutive theory is displayed in an abstract way to allow a straightforward presentation from a 3D perspective. Such an approach is essential to the development of the final governing equations of the model (in Section 4) and accurate expressions for the rate of energy dissipation (in Section 5).

The thermodynamic state of an anelastic solid is supposed to be identified by the total and anelastic strains tensors $\boldsymbol{\varepsilon}$, and $\boldsymbol{\varepsilon}^a$, in addition to a set of internal variables, denoted abstractedly as β. Without loss of generality from now on, β is assumed to be a scalar variable. The Helmholtz free energy potential Ψ is assumed to be an additive decomposition of elastic and anelastic strain energy densities W_e and W_a, respectively

$$\rho_p \Psi(\,\boldsymbol{\varepsilon},\; \boldsymbol{\varepsilon}^a,\; \beta) = \mathrm{W}_e\; + \mathrm{W}_a, \tag{14}$$

where ρ_p is the mass density of the material, which is supposed to be constant, with W_e being a classical function of the elastic deformation $(\boldsymbol{\varepsilon} - \boldsymbol{\varepsilon}^a)$ of the material. As usual, the elastic strain energy density is conceived as [41]:

$$\mathrm{W}_e = \frac{1}{2}\mathbf{C}[(\boldsymbol{\varepsilon} - \boldsymbol{\varepsilon}^a) : (\boldsymbol{\varepsilon} - \boldsymbol{\varepsilon}^a)]\,. \tag{15}$$

Here " : " represents the inner product of tensors, i.e., $\mathbf{A}$: $\mathbf{B} = \mathrm{tr}(\mathbf{A}^{\mathrm{T}}\mathbf{B})$. In Eq. (15), $\mathbf{C}$ stands for the classic symmetric, positive-definite fourth-order tensor of the elasticity theory and $\mathrm{W}_a = \mathrm{W}_a(\beta)$ is supposed to be a differentiable function of the internal variable β. The thermodynamic forces $\boldsymbol{\sigma}$ and B^β are obtained by taking the partial derivatives of the Helmholtz potential with respect to the state variables $(\boldsymbol{\varepsilon},\; \boldsymbol{\varepsilon}^a, \beta)$ [42]:

$$\boldsymbol{\sigma} = \rho_p \frac{\partial \Psi}{\partial \boldsymbol{\varepsilon}} = \rho_p \frac{\partial \mathrm{W}_e}{\partial \boldsymbol{\varepsilon}} = \rho_p \frac{\partial \mathrm{W}_e}{\partial (\boldsymbol{\varepsilon} - \boldsymbol{\varepsilon}^a)}, \tag{16}$$

$$\mathrm{B}^\beta = -\rho_p \frac{\partial \Psi}{\partial \beta} = -\rho_p \frac{\partial \mathrm{W}_a}{\partial \beta}. \tag{17}$$

Equation (16) is the usual relationship that describes the purely elastic response, whereas Eq. (17) describes the reversible parcel associated with the anelastic behavior of the material. Such state laws are still insufficient to fully describe the anelastic behavior since the relationships between the internal variable, β, and the tensors $\boldsymbol{\varepsilon}^a$ and $\boldsymbol{\sigma}$ are still unknown. This task is completed by introducing a scalar-differentiable pseudo-potential of dissipation $\Phi\,(\boldsymbol{\sigma},\; \mathrm{B}^\beta)$, from which the evolution laws are derived by taking their partial derivatives as such [42]

$$\dot{\boldsymbol{\varepsilon}}^a = \frac{\partial \Phi}{\partial \boldsymbol{\sigma}}, \tag{18}$$

$$\dot{\beta} = \frac{\partial \Phi}{\partial \mathrm{B}^\beta}, \tag{19}$$

where superimposed dot means partial derivative with respect to time. If the pseudo-potential of dissipation Φ is convex, positive, and null at the origin, then it can be proved that the rate of energy dissipation in the material is always positive, as will be exposed in Section 5.2. In other words, the model obeys unconditionally the second law of thermodynamics (SLT). Therefore, the choice of pseudo-potential based on the restrictions imposed in the prior statement and the proper anelastic

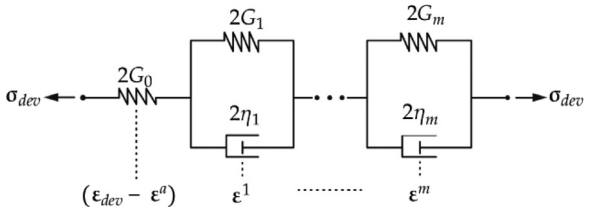

Fig. 2. Sketch of the generalized Kelvin-Voigt model. The variable ε_{dev} stands for the deviatoric parcel of the total strain ε.

strain energy provide the final form of the set of consistent thermodynamic equations that formulates the constitutive behavior of an anelastic material.

The mechanical behavior of the pipe material is assumed to be described by linear viscoelasticity. As usual, linear viscoelasticity can be described from mechanistic models. As experimental findings in solid-like viscoelastic materials, such as the ones used in pipes, are better tracked when the mechanistic model describes an elastic and instantaneous response followed by an asymptotic viscoelastic response, the so-called generalized Kelvin-Voigt model turns out to be a suitable choice. In addition to properly characterizing polymeric materials used in pipes, under the present constitutive theory the generalized Kelvin-Voigt model renders a simple pseudo-potential of dissipation that ensures a thermodynamically consistent model, as presented in Section 5.2. Thence, the rates of energy dissipation in the pipe material, a feature largely explored in the present work, can be easily assessed and computed.

By assuming that the pipe mechanical response is merely deviatoric, the generalized Kelvin-Voigt model is formed by m units of Kelvin-Voigt elements, with shear elastic constants G_i and coefficients of viscosity $\eta_i\,(i = 1, \ldots, m)$, coupled in series with a spring with an instantaneous shear modulus of elasticity G_0 is considered. Each of these Kelvin-Voigt units is associated with a second-order strain tensor $\boldsymbol{\varepsilon}^i\{\ i = 1, \ldots, m\}$ so that the anelastic strain tensor $\boldsymbol{\varepsilon}^a$ is equal to the summation over i of $\boldsymbol{\varepsilon}^i$. A sketch of this mechanical model is shown in Fig. 2.

Based on the sketch shown in Fig. 2, the set of state variables for this viscoelastic material can be identified as:

$$(\boldsymbol{\varepsilon},\ \boldsymbol{\varepsilon}^a,\ \beta) \text{ with } \beta = \boldsymbol{\varepsilon}^i,\ \text{such that } \boldsymbol{\varepsilon}^i = \boldsymbol{\varepsilon}^i_{dev} \text{ and } \boldsymbol{\varepsilon}^a = \sum_{i=1}^{m} \boldsymbol{\varepsilon}^i. \tag{20}$$

Assuming that the pipe material is isotropic, the particular forms of the anelastic strain energy density and the pseudo-potential of dissipation become [43]

$$\mathrm{W}_a = \sum_{i=1}^{m} \frac{1}{2}\left[\frac{2}{3}\, E_i\, \boldsymbol{\varepsilon}^i : \boldsymbol{\varepsilon}^i\right], \tag{21}$$

$$\Phi = \sum_{i=1}^{m} \frac{1}{2}\left[\frac{3}{2}\frac{1}{E_i\tau_i}\left(\mathbf{B}^{\boldsymbol{\varepsilon}^i} + \boldsymbol{\sigma}_{dev}\right) : \left(\mathbf{B}^{\boldsymbol{\varepsilon}^i} + \boldsymbol{\sigma}_{dev}\right)\right], \tag{22}$$

where $\tau_i = \eta_i/G_i$ and $E_i = 3G_i$ are the relaxation time and Young's modulus of the $i-th$ Kelvin-Voigt unit, and $\boldsymbol{\sigma}_{dev}$ represents the deviatoric part of the tensor $\boldsymbol{\sigma}$. Taking into account Eq. (16-17), the preceding anelastic energy density gives rise to the following state laws:

$$\boldsymbol{\sigma} = \rho_p \frac{\partial \mathrm{W}_e}{\partial(\boldsymbol{\varepsilon} - \boldsymbol{\varepsilon}^a)} = \frac{\nu_0}{(1+\nu_0)}\ \mathrm{tr}\ \boldsymbol{\sigma} + \frac{E_0}{(1+\nu_0)}(\boldsymbol{\varepsilon} - \boldsymbol{\varepsilon}^a), \tag{23}$$

$$\mathbf{B}^{\boldsymbol{\varepsilon}^i} = -\rho_p \frac{\partial \mathrm{W}_a}{\partial \boldsymbol{\varepsilon}^i} = -\frac{2}{3} E_i \boldsymbol{\varepsilon}^i \text{ for } i = 1, \ldots, m, \tag{24}$$

where E_0 and ν_0 are the instantaneous Young's modulus and Poisson's ratio. The pseudo-potential of dissipation given in Eq. (22) gives rise to the following evolution laws:

$$\dot{\boldsymbol{\varepsilon}}^i = \frac{\partial \Phi}{\partial \mathbf{B}^{\boldsymbol{\varepsilon}^i}} = \frac{3}{2}\frac{1}{E_i\tau_i}\left(\boldsymbol{\sigma}_{dev} + \mathbf{B}^{\boldsymbol{\varepsilon}^i}\right) = \frac{3}{2}\frac{\boldsymbol{\sigma}_{dev}}{E_i\tau_i} - \frac{\boldsymbol{\varepsilon}^i}{\tau_i},\ \text{for } i = 1, \ldots, m, \tag{25}$$

$$\dot{\boldsymbol{\varepsilon}}^a = \frac{\partial \Phi}{\partial \boldsymbol{\sigma}} = \sum_{i=1}^{m}\left[\frac{3}{2}\frac{1}{E_i\tau_i}\left(\boldsymbol{\sigma}_{dev} + \mathbf{B}^{\boldsymbol{\varepsilon}^i}\right)\right] = \sum_{i=1}^{m} \dot{\boldsymbol{\varepsilon}}^i\ . \tag{26}$$

This formulation comprises the description of creep and relaxation phenomena that are present in standard viscoelastic materials: the instantaneous purely elastic response of the material Eq. (23)) is followed by a time-dependent anelastic response (Eqs. (25-(26)). It is worth noting that the Poisson's ratio in the present model presents an elastic and instantaneous response followed by a time-dependent one, which can be computed by the ratio of the transverse and longitudinal

strain responses of the model obtained from a creep compliance test, ε_{22} and ε_{11}, with the use of Eqs. (23-26), so that $\nu(t) = -\varepsilon_{22}(t)/\varepsilon_{11}(t)$. Thus, even though not addressed explicitly as in Keramat et al. [44–45], the time-dependent nature of Poisson's ratio is captured in the model.

By appealing to the constitutive equations given in Eqs. (23-26), the proposed viscoelastic model is fully characterized when the values of the material parameters ν_0, E_0, and (τ_i, E_i), for $i = 1, \ldots m$, are addressed. As pointed out by Weinerowska-Bords [46–47], the set of parameters (τ_i, E_i, m) does not hold physical meaning as such, except when the resulting creep compliance curve of the material is considered. Two distinct approaches may be used to achieve these material constants: i) via mechanical tests (creep, relaxation, or dynamical loading essays) in a specimen from a sample of the pipe material; or ii) through calibration strategies, based on collected transient data using a fluid-transient solver which takes into account both the pipe-wall viscoelasticity and the unsteady friction (UF) - the main phenomena responsible for attenuation and dispersion of the pressure responses [12,48-49]. In the present work, the model adopted the Kelvin-Voigt parameters achieved by the first approach for all experimental installations from which pressure measurements were extracted to further compare with the model's responses. Such a strategy avoids some of the uncertainties associated with the determination of the Kelvin-Voigt parameters [12,44,46-47].

4. Governing equations

The model's governing equations are obtained by combining the balance equations Eqs. (1-(3)) with the respective constitutive equations for fluid Eqs. (4-(5)) and pipe Eqs. (23-(26)). The fluid constitutive equations are ready to be incorporated, but the constitutive pipe relations are still quite general.

In the present work, the pipe is subjected to internal pressure loads only. As a result, the circumferential stress σ_θ turns out to be the only independent one among the principal stresses of the tensor $\boldsymbol{\sigma}$. Furthermore, the deviatoric part of the stress, which is present in the evolution laws of the material Eqs. (25-(26)), is assumed to be approximated by a quasi-static stress distribution. In contrast to the majority of metallic pipes, polymeric pipes which exhibit viscoelastic behaviors are generally manufactured as thick-walled pipes, with radius-to-thickness ratios in the range $R/e < 10$. Thus, the radial stress component σ_r may become significant and therefore cannot be carelessly disregarded, as in the classic thin-walled tube theory. To cope with thick-walled pipes, averaged values of axial, circumferential and radial stresses based on the quasi-static stress distribution of a ring (or hoop) subjected to internal pressure loads as derived by Tijsseling [50] are employed. Meanwhile, as the pipe's inertia is assumed to be negligible, the axial stress is simply given by $\sigma_x = \nu_0(\sigma_\theta + \sigma_r)$.

Based on these assumptions, the set of evolution laws of the material turns out to be in terms of cross-sectional averages. Thus, the term related to the anelastic circumferential strain at the internal pipe radius in the mass-balance equation of the fluid must be altered to account for averaged values. The development of the final mass-balance equation is presented in Appendix B. With this in mind, the governing equations of the mechanical model for the unknowns $p,\ v,\ v_2,\ \ldots, v_n,\ \varepsilon_\theta^a,\ \varepsilon_\theta^1,\ \ldots \varepsilon_\theta^m$ are given by:

$$\left(\frac{1}{\rho_0 c_f^2}\right)\frac{\partial p}{\partial t} + \frac{\partial v}{\partial x} + 2\Pi\frac{\partial \varepsilon_\theta^a}{\partial t} = 0, \tag{27a}$$

$$\frac{\partial v}{\partial t} + \frac{1}{\rho_0}\frac{\partial p}{\partial x} + \frac{2}{R\rho_0}a_n = 0, \tag{27b}$$

$$\frac{\partial v_j}{\partial t} + \frac{1}{\rho_0}\frac{\partial p}{\partial x} + \frac{1}{\alpha_j\rho_0}\left(m_j + \frac{2}{R}a_j\right) = 0,\ j = 2,\ \ldots,\ n, \tag{27c}$$

$$\frac{\partial \varepsilon_\theta^a}{\partial t} + g_\theta = 0, \tag{27d}$$

$$\frac{\partial \varepsilon_\theta^i}{\partial t} + g_i = 0, \tag{27e}$$

where

$$c_f = \left\{\rho_0\left[\frac{1}{K} + \frac{2}{E_0}\left\{\frac{R}{e} + \frac{\left(1+\frac{e}{R}\right)}{\left(2+\frac{e}{R}\right)} + \nu_0 - \nu_0^2\Gamma\right\}\right]\right\}^{-1/2}, \tag{28}$$

is the pressure wavefront speed, and

$$g_\theta = -\left(\sum_{i=1}^{m}\frac{1}{2}\frac{(\Omega - \nu_0\Gamma)p}{E_i\,\tau_i} - \frac{\varepsilon_\theta^i}{\tau_i}\right), \tag{29a}$$

$$g_i = -\left(\frac{1}{2}\frac{(\Omega - \nu_0\Gamma)p}{E_i\,\tau_i} - \frac{\varepsilon_\theta^i}{\tau_i}\right),\ i = 1,\ \ldots,\ m, \tag{29b}$$

$$\Pi = \frac{2\left(R + \frac{1}{2}e\right)}{R}, \tag{29c}$$

$$\Gamma = (\sigma_\theta + \sigma_r)/p = \frac{R}{e}\frac{1}{1+\frac{1}{2}\frac{e}{R}}, \text{ and} \tag{29d}$$

$$\Omega = (2\sigma_\theta - \sigma_r)/p = \frac{R^2}{e(e+2R)} + \frac{6R^2(e+R)^2\ln\left[1+\frac{e}{R}\right]}{e^2(e+2R)^2}. \tag{29e}$$

Equations (27a) and (27b) are the balances of mass and linear momentum for the virtually structured mixture as a whole, respectively, and Eq. (27c) represents the balances of the axial momentum for each constituent. Equations (27d,27e) are the evolution laws of the material. With the introduction of the anelastic strain and its evolution laws, the model can handle both the elastic and viscoelastic behavior of the pipe. The elastic model, which ignores the pipe's viscoelasticity, is obtained by eliminating the anelastic strain terms in the balance of mass and their respective evolution laws.

5. Rate of energy dissipation

5.1. Fluid

The rate of energy dissipation in the liquid is readily computed with the aid of the theory of mixtures in which the fluid model has been developed. This theory enforces the second law of thermodynamics to be postulated for each constituent as well as for the mixture as a whole [51]. Based on the assumptions made so far, and assuming that the sole mechanism of energy dissipation is due to the momentum transfer among the constituents, the second law of thermodynamics for each constituent is stated as

$$d_j = a_j \nu_j \frac{P}{A} \geq 0, \tag{30}$$

while for the mixture as a whole, the SLT is expressed as

$$d_m = \sum_{j=1}^{n} m_j \nu_j \geq 0. \tag{31}$$

The thermo-mechanics of the pseudo-mixture allows one to conclude that the summation of all parcels presented in Eqs (30-31) is the overall energy dissipation in the fluid flow. With the aid of the mixture constitutive equations Eqs. 4-(5), the rate of energy dissipation d_f in the fluid becomes:

$$d_f = \sum_{j=1}^{n} d_j + d_m = \sum_{j=1}^{n} C_{j,j+1}\left(\nu_{j+1} - \nu_j\right)^2 + \frac{2}{R}C(\nu_n)^2. \tag{32}$$

5.2. Pipe

Assuming that the pipe is subjected to isothermal processes, the local form of the second law of thermodynamics (SLT), which states that the rate of energy dissipation in the pipe per unit volume, d_p, must be non-negative, can be stated as [35–36]:

$$d_p = \boldsymbol{\sigma} : \dot{\boldsymbol{\varepsilon}} - \rho_p \dot{\Psi} \geq 0. \tag{33}$$

By taking Eqs. (23-26) into account, Eq. (33) can be expressed as the following

$$d_p = \boldsymbol{\sigma} : \frac{\partial \Phi}{\partial \boldsymbol{\sigma}} + \sum_{i=1}^{m} \mathbf{B}^{\boldsymbol{\varepsilon}^i} : \frac{\partial \Phi}{\partial \mathbf{B}^{\boldsymbol{\varepsilon}^i}} \geq 0. \tag{34}$$

Finally, when the expressions of the state and the evolution laws established in Eqs. (23-26) are considered, the local rate of energy dissipation in the viscoelastic material can be written as

$$d_p = \sum_{i=1}^{m} \left(\boldsymbol{\sigma}_{dev} + \mathbf{B}^{\boldsymbol{\varepsilon}^i}\right) : \dot{\boldsymbol{\varepsilon}}^i \geq 0. \tag{35}$$

Hence, d_p can be readily computed in terms of the dependent variables of the proposed model p and $\varepsilon_\theta^1, \ldots, \varepsilon_\theta^m$ as (see Section 4):

$$d_p = \sum_{j=1}^{m} \frac{2}{3} E_i \tau_i \left(\dot{\varepsilon}_\theta^i\right)^2 = \sum_{j=1}^{m} \frac{2}{3} E_i \tau_i (g_i)^2 \geq 0. \tag{36}$$

As E_i and τ_i are positive constants, Eq. (36) is always non-negative and therefore the proposed model satisfies unconditionally the second law of thermodynamics. It is worth noting that the constitutive equations used herein are based on a mathematical generalization of sufficient conditions imposed on the pseudo-potential of dissipation Φ so that the modeling is thermodynamically consistent. In effect, as Φ is convex, positive, and null at the origin, the inequality presented in Eq. (34) follows a classical result from the convex analysis [35,52], which can be expressed in a compact form as:

$$d_p = \boldsymbol{\sigma} : \frac{\partial \Phi}{\partial \boldsymbol{\sigma}} + \sum_{i=1}^{m} \mathbf{B}^{\boldsymbol{\varepsilon}^i} : \frac{\partial \Phi}{\partial \mathbf{B}^{\boldsymbol{\varepsilon}^i}} \;\geq\; \Phi \;\geq\; 0. \tag{37}$$

Thus, the result of non-negative dissipative processes is ensured a priori in the present constitutive theory.

6. Numerical procedure

The mechanical model represented by Eq. (27) forms a quasi-linear hyperbolic system of partial differential equations. Applying the method of characteristics for this system produces the following set of compatibility equations (see Appendix C):

$$\frac{1}{\rho_0\, c_f}\frac{dp}{dt} + \frac{dv}{dt} = -\frac{2}{R\rho_0}a_n + 2c_f \Pi g_\theta \text{ along } C^+ \equiv \frac{dx}{dt} = c_f, \tag{38a}$$

$$-\frac{1}{\rho_0\, c_f}\frac{dp}{dt} + \frac{dv}{dt} = -\frac{2}{R\rho_0}a_n - 2c_f \Pi g_\theta \text{ along } C^- \equiv \frac{dx}{dt} = -c_f, \tag{38b}$$

$$-\frac{dv}{dt} + \frac{dv_j}{dt} = -\frac{m_j + \frac{2}{R}a_j}{\rho_0 \alpha_j} + \frac{2}{R\rho_0}a_n \text{ for } j = 2, \ldots n, \text{ along } C^0 \equiv \frac{dx}{dt} = 0, \tag{38c}$$

$$\frac{d\varepsilon_\theta^a}{dt} = -g_\theta \text{ along } C^0 \equiv \frac{dx}{dt} = 0, \tag{38d}$$

$$\frac{d\varepsilon_\theta^i}{dt} = -g_i;\; i = 1, \ldots, m, \text{ along } C^0 \equiv \frac{dx}{dt} = 0, \tag{38e}$$

in which g_θ and g_i are defined in Eq. (29) and the characteristic equations of the model C^+,C^-,$C^0$are defined by the eigenvalues of the problem $+c_f$,$-c_f$, and 0, respectively.

The two non-null eigenvalues are related to the characteristic curves through which perturbations propagate in the domain. Meanwhile, the null eigenvalues are associated with the characteristics responsible for dispersive and/or dissipative effects. Such physical phenomena take place in both the liquid and pipe and are due to friction and turbulence in the fluid and anelastic circumferential deformations of the pipe.

To obtain approximated solutions for the initial-boundary-value problem governed by Eq. (38), an integration process must be carried out along those characteristic curves. To achieve this goal, a discrete grid of the independent variables must be employed by considering a temporal-spatial discretized domain in which $x_k = (k-1)\Delta x$ and $t_p = t_{p-1} + \Delta t$, for $k = 1$, ..., $N+1$ and $p = 1, 2, \ldots$, with $t_0 = 0$, $\Delta x = L/N$ and $\Delta t = \Delta x/c_f$. Within this choice of the discrete spatial-temporal grid, the Courant-Friedrichs-Levy (CFL) stability condition, $\Delta t \leq \Delta x/c_f$, is automatically satisfied and the compatibility equations can be integrated in the $t-x$ plane along the characteristic curves, for $k = 2, \ldots, N$ according to the stencil depicted in Fig. 3.

As the stencil ties all characteristic curves, the approximations of $\mathbf{U} = [p,\ v,\ v_j\{j = 2, \ldots n\},\ \varepsilon_\theta^a,\ \varepsilon_\theta^i\{i = 1, \ldots m\}]$ at the discrete points (x_k, t_p) may readily be computed. This procedure allows calculating $\mathbf{U}$ at the time instant $t_p = t_{p-1} + \Delta t$ by invoking the prior value of $\mathbf{U}$ at t_{p-1} for $k = 2, \ldots, N$, with $t_0 = 0$ being the time instant representative of a known steady-state solution of Eq. (27).

The integration procedure of the left-hand sides of the compatibility equations is exact. On the other hand, that of the right-hand sides of Eqs. (38a-d) are evaluated by employing an implicit second-order (Crank-Nicholson) approximation for the terms a_j, m_j, and g_θ. In addition, a discretized form of the compatibility equations represented by Eq. (38e) can be obtained by direct integration of these equations, when weighted by $\exp(t/\tau_i)$ followed by an explicit first-order approximation of the pressure variable p. Besides the time-spatial discretization, the number and thickness of the constituents must be specified since it is a constitutive choice in the context of the model. In this work, the thickness of each constituent is maintained constant in a core region ($0 \leq R_j \leq 0.8R$), while the thicknesses of the constituents in the annular region ($0.8R < R_j \leq R_n$) decrease following a geometric progression. Details of this constituents' grid can be found in Andrade and Freitas Rachid [37].

The discretized equations with appropriate initial-and-boundary conditions form a linear system of equations whose solution, i.e. the vector of unknowns $\mathbf{U} = [p,\ v,\ v_j\{j = 2, \ldots n\},\ \varepsilon_\theta^a,\ \varepsilon_\theta^i\{i = 1, \ldots m\}]$ at each discretized time-space node (x_k, t_p), is obtained by employing a Householder reduction followed by back substitution.

The approximate solution for the case that the pipe wall is linearly elastic, which is analyzed in the next section as well, can be achieved by the same general procedure as described above. Nevertheless, the final set of equations to be solved is

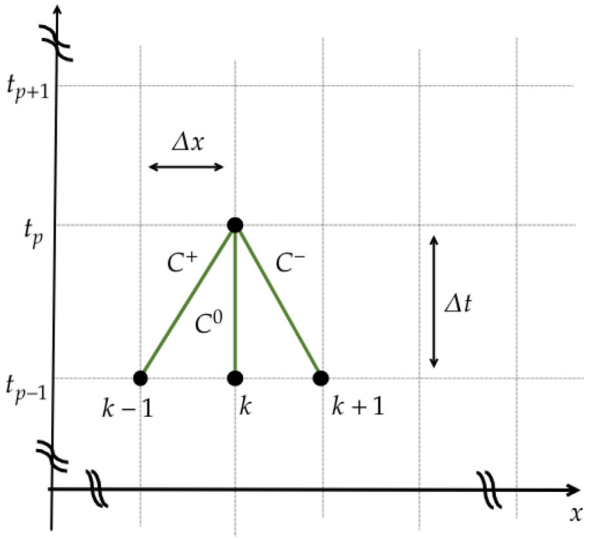

Fig. 3. Computational mesh based on characteristic curves for the present model.

limited to only $n + 1$ dependent variables $[p,\ v,\ v_2 \ldots v_n]_{n+1}$. Then, the model turns out to be equal to the one presented by Andrade and Freitas Rachid [37], which is valid for elastic pipe materials.

7. Results

Before going a step further aiming to explore the full capabilities of the proposed model, we validate the model by comparing its numerical predictions with experimental results available in the literature. The accuracy of the model is assessed by comparing the numerical results of the piezometric head, H, fluctuations next to the valve, with the data found in two experimental installations: of Gally et al. [8] and Covas [53]. Their experimental apparatus is composed of a reservoir from which water flows at a steady-state velocity v_0 in a horizontal polymeric pipe that reaches a downstream-end valve located at $x = L$. Initially, this valve is fully open, and then the transient is generated by a rapid valve closure maneuver within closure time $\mathcal{T}$ The following boundary conditions mathematically describe this settlement:

$$H(x = 0, t) = H_R(t), \tag{39}$$

$$v(L, t) = \begin{cases} v_0\left(1 - \dfrac{t}{\mathcal{T}}\right) & \text{if } 0 \le t < T \\ 0 & \text{if } t \ge T \end{cases}, \tag{40}$$

in which $H_R(t)$ is the reservoir pressure.

Three cases, referred to as Cases (1), (2) and (3), will be considered in this work. The first two are referred to as the experimental cases of Covas [53], and the third one is related to the experiment conduced by Gally et al. [8]. In the first, the flow regime is laminar, while, in the other two, it is turbulent. The main features of the experimental setup for Covas' cases can be found in Table 1, and the viscoelastic characteristics of the HDPE tube employed in the experimental facility of Covas [53] are specified in Table 2. Tables 3 and 4 display the features of the experimental apparatus and the details of the

Table 1
Main characteristics of the experiment of Covas [53].

Case	L[m]	D[m]	e [m]	$\rho_0[\frac{\text{kg}}{\text{m}^3}]$	$\nu_0[-]$	$c_f[\frac{m}{s}]$	$\mathcal{T}$ [s]	$v_0\,[\frac{\text{m}}{\text{s}}]$	Re [−]	$H_R(t(s))$[m]
1	271.5	0.0506	0.00625	998.2	0.46	394	0.13	0.028	1398	$48.33 + 0.0167t - 0.0004t^2$
2								0.25	12581	$46.95 + 0.115t - 0.0035t^2$

Table 2
Coefficients of the Kelvin-Voigt units of the HDPE tube of Covas [53] (Covas et al. [49]).

Unit	$i = 1$	$i = 2$	$i = 3$	$i = 4$	$i = 5$
$E_i[10^9\text{Pa}]$	7.17	161.29	8.71	2.92	10.78
τ_i[s]	0.05	0.5	1.5	5	10

Table 3
Main characteristics of the experiments of Gally et al. [8] (Urbanowicz et al. [54]).

Case	L[m]	D[m]	e [m]	$\rho_0[\frac{kg}{m^3}]$	$\nu_0[-]$	$c_f[\frac{m}{s}]$	$\mathcal{T}$ [s]	$v_0[\frac{m}{s}]$	Re [−]	$H_R(t(s))$[m]
3	43.1	0.0416	0.0042	997.1	0.38	265	0.012	0.55	25650	10.89

Table 4
Coefficients of the Kelvin-Voigt units of the Polyethylene (PE) tube of Gally et al. [8] – temperature equal to 25°C (Urbanowicz et al. [21]).

Unit	$i = 1$	$i = 2$
$E_i[10^9 Pa]$	0.9560	0.8084
$\tau_i[s]$	0.0222	1.864

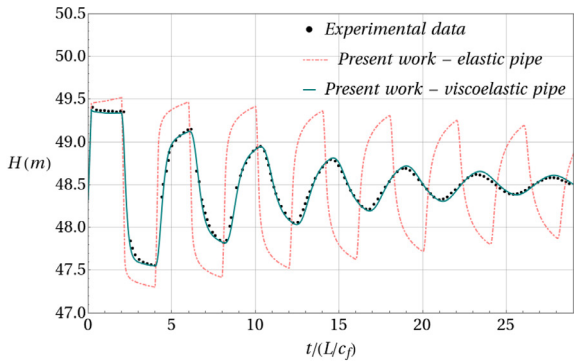

(a)

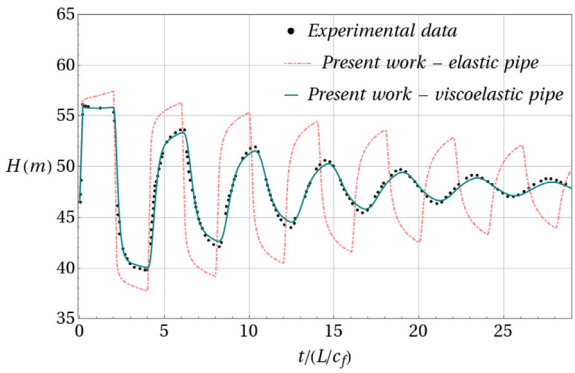

(b)

Fig. 4. Piezometric head histories located at 0.5 m upstream of the valve extracted from the experimental data of Covas [53]. Comparison between the present model by considering the pipe-wall mechanical behavior as being viscoelasticity and elastic. Figs. (a) and (b) refer to Case (1) and Case (2), respectively.

polyethylene pipe employed by Gally et al. [8], as reported by Urbanowicz et al. [21,54]. As one can see in the right-most column of Table 1, the reservoir head function for Covas' experiments (Cases (1) and (2)) is approximated by time-dependent functions for both the laminar and turbulent cases. These functions are extracted from the reservoir pressures registered in Covas [53] for the turbulent case, while due to the absence of these pressure traces for the laminar flow case in the work of Covas [53], the function for the laminar flow case was extracted from the reservoir pressures exposed by Urbanowicz et al. [55]. The reservoir pressure as being a function of time t in the experiments carried out by Covas [53] is also remarked by Abdel-Gawad and Djebdjian [56]. The reservoir pressure in Case (3) is assumed to be constant (see Table 3).

Figs. 4 and 5 show the transient piezometric head histories close to the valve for both laminar and turbulent cases obtained by the present approach together with experimental data obtained by Covas [53] and Gally et al. [8]. To enrich the analysis, the present model responses disregarding the effects of the viscoelasticity of the pipe (elastic pipe model) are also presented in Figs. (4) and (5). As one can see, the elastic model is unable to properly represent the experimental data. This model overestimates the values of the head for the whole time span and is not in phase with the experimental responses.

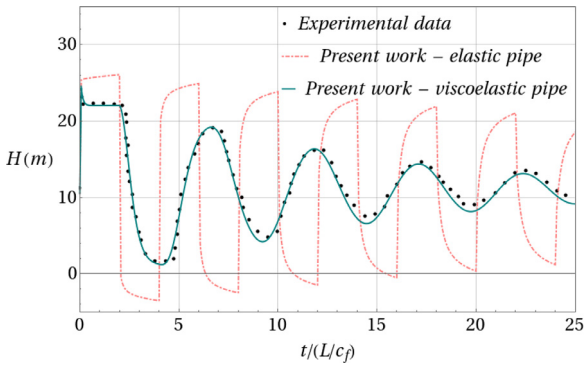

Fig 5. Piezometric head histories located next to the downstream valve extracted from the experimental data of Gally et al. [8] for temperature equal to 25°C. Comparison between the present model by considering the pipe-wall mechanical behavior as being viscoelastic and elastic.

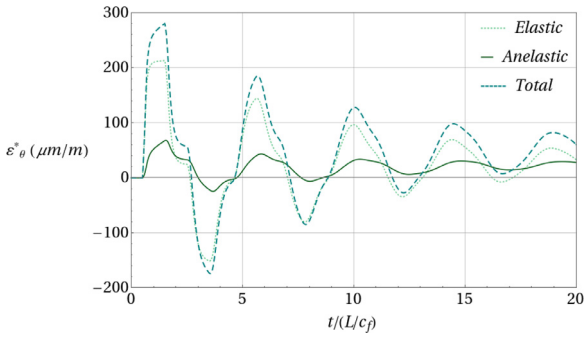

Fig. 6. Relative circumferential strain histories computed by the present model when viscoelastic response is taken into account at the mid-length of the viscoelastic pipe for the experimental setup of Covas [53]. The elastic and anelastic parcels of the relative circumferential strain are also presented.

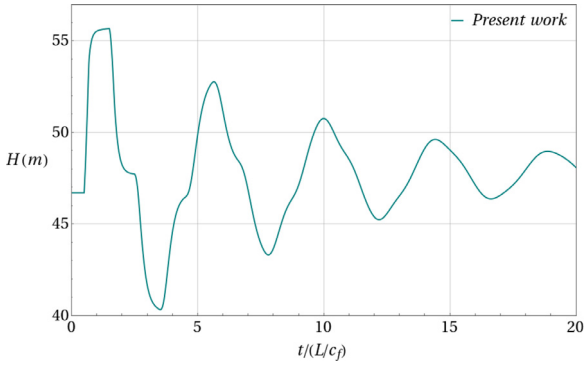

Fig. 7. Piezometric head histories at the mid-length of the viscoelastic pipe computed by the present model when the viscoelasticity is taken into account for the experimental setup of Covas [53].

Conversely, the proposed viscoelastic model responses agree quite well both in phase and magnitude with the experimental data.

The differences between the piezometric heads predicted by the model with the elastic and viscoelastic pipe wall mechanical behaviors can be better comprehended by analyzing some intrinsic aspects of this material's behavior. Case (2) is selected to present such an analysis, even though it could have been done with Cases (1) and (3) as well.

Fig. 6 shows the relative total strain ε_θ for the viscoelastic response (the difference between the current and initial state, i.e. $\varepsilon^*_\theta = \varepsilon_\theta - \varepsilon_\theta|_{t=0}$) and its anelastic parcel and elastic counterpart at the mid-length of the pipe.

The behavior of anelastic strains through time due to the cyclic wave passages at a particular position differs from that of the elastic strains. Meanwhile, the elastic strain has an instantaneous response to the pressure loads, the anelastic strain is characterized by a delayed response. For example, after the passage of the first wavefront at the pipe mid-length at $t/(L/c_f) \cong 0.5$, the elastic strain and piezometric head are roughly held constant until the subsequent wavefront arrival at $t/(L/c_f) \cong 1.5$ (see Figs. 6 and 7). In contrast, the anelastic strains increase significantly in this whole period. In other words,

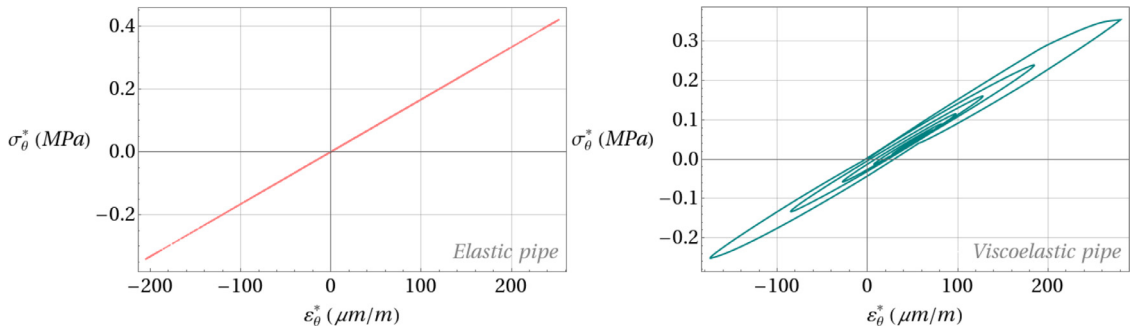

Fig. 8. Relative stress-strain hysteresis curves at the mid-length of the pipe during $t/(L/c_f) \in [0,\ 29]$ for the experimental setup of Covas [53].

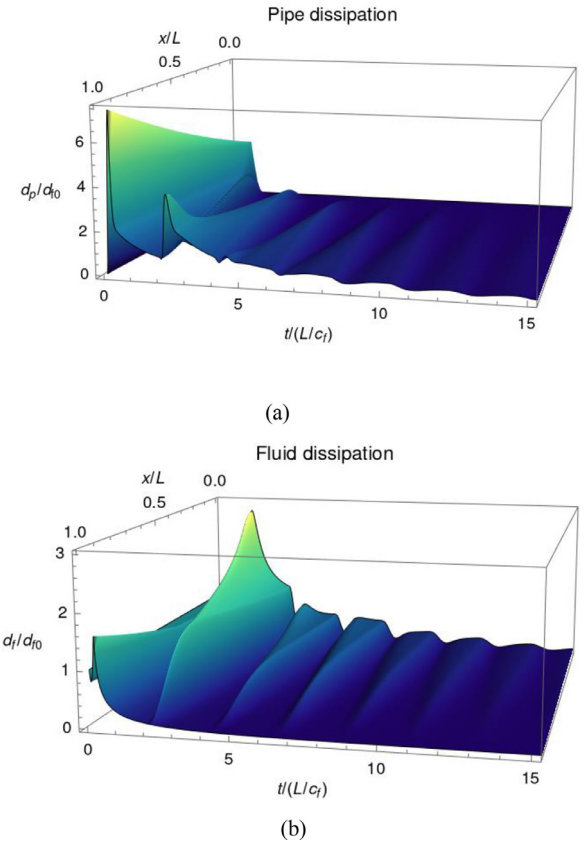

Fig. 9. Normalized local rates of energy dissipation in the (a) pipe and the (b) fluid for the experimental setup of Covas [53].

the pressure and anelastic strain are not in phase, as has already been noticed by Pezzinga et al. [14]. This increase of the anelastic strain at a constant pressure/stress load is known as creep. This strain is a consequence of internal rearrangements of the pipe material's structure that is captured by the internal variables ε^i_θ. Such a delayed material response causes mechanical hysteresis, which is a typical evidence of energy dissipation. Fig. 8 shows the difference between the current and initial stress ($\sigma^*_\theta = \sigma_\theta - \sigma_\theta|_{t=0}$) against the relative total strain during the normalized time interval $t/(L/c_f) \in [0,\ 29]$. In contrast to the response of the elastic pipe, hysteresis is observed in the viscoelastic pipe, as the loading and unloading processes do not follow the same path in the $\sigma^*_\theta - \varepsilon^*_\theta$ plane. Such behavior is directly related to the delayed strain responses to the pressure loads that are observed in viscoelastic pipes.

Since hysteresis is intrinsically related to energy dissipation phenomena, to better grasp the influence of the viscoelasticity on the dynamic response of the pipe-fluid system, it is convenient to keep track of the rate of energy dissipation in both the pipe and fluid.

Fig. 9 shows histories of the local rate of energy dissipation per unit volume in the fluid and the pipe normalized by the local rate of energy dissipation in the fluid in the steady-state d_{f0}. In the present case, the liquid's dissipation and the

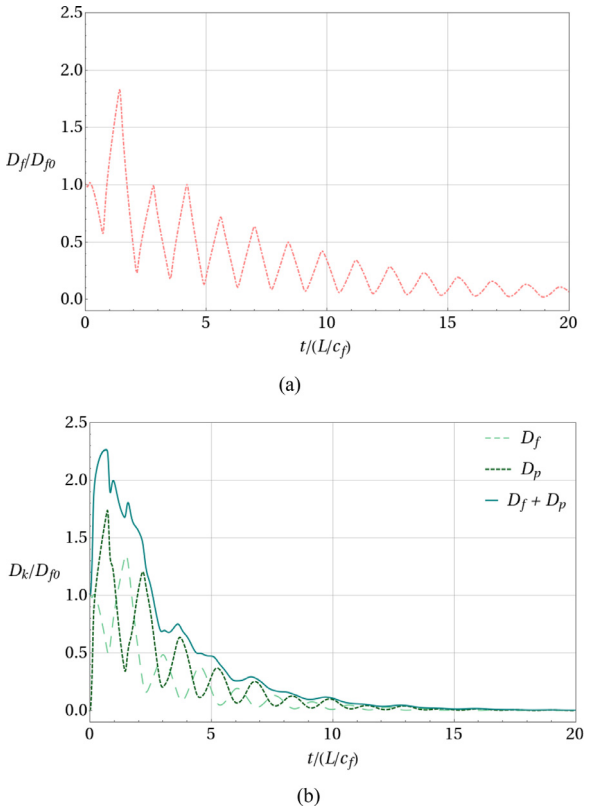

Fig. 10. Normalized overall rate of energy dissipation in both fluid and pipe through the pipe extension. Comparison between the responses of the present model: (a) elastic and (b) viscoelastic tube materials. In (b), the summation of the dissipation in both media is also shown.

solid's dissipation have the same order of magnitude, being the solid energy dissipation more prominent. Further, Fig. 9 also reveals that the dissipation in the pipe takes place at the very first moments of the transient and is localized in regions close to the valve. The rapid and intense pressure surge right after the onset of the transient induces a significant amount of anelastic strains, which in turn are directly associated with dissipative phenomena (see Eq. 36). Such evidence supports the employment of short viscoelastic pipe sections in elastic pipelines to act as pressure surge suppressors, especially when these additional pipes are placed close to the source of the transient [25–32].

As pressure surges also enforce flow reversals, the no-slip condition at the pipe wall ends up creating uneven velocity gradients. Since the velocity gradients are decisive for liquid dissipation in transients and are more severe at the onset of these events, the dissipation in the fluid achieves its more pronounced values in the first moments. However, the shape of the distribution of the rates of energy dissipation is more complex than the pattern found in pipe dissipation. Such a result is due to intricate patterns and intensities of the flow reversals at different time instants [57–58]. In the present case, it is noted that the more significant values of rates of energy dissipation in the fluid are observed in regions close to the reservoir, especially when the fluid wavefront attains these locations at $t/(L/c_f \cong 1)$. Right after $t/(L/c_f \cong 1)$, the flow still maintains its inertia and starts to reverse completely its direction from the reservoir towards the valve. As a consequence, significant reverse flows close to the wall appear, and high levels of rates of energy dissipation in the fluid arise from them.

The preceding paragraphs expose that even though fluid and pipe energy dissipations contribute to the attenuation and dispersion of the pressure oscillations, each media has its proper mechanics that act differently during transients. Such a result contributes to one of the main challenges of the field, as Covas et al. [49] stated: "The major challenge of the current and the future work is the distinction between frictional and mechanical dampening." In Covas et al. [49] and other subsequent works, as in Duan et al. [12] and Seck [59], the strategy to observe the impact of the fluid transient friction and viscoelastic in the fluid transient is based on computing the model's responses by taking into account only one of these two effects and observe a local pressure response close to the valve. Even though the effect of the viscoelasticity seems to be more significant as it achieved close results to experimental data, in both cases, the pressure signals are attenuated and dispersed similarly. Thus, from the pressure results, it is impossible to discern the exact effects of each medium on the pressure responses when they are combined in the model.

On the other hand, the present approach, which describes the computation of the local rates of energy dissipation in both media separately, clearly contributes to the distinction and mechanical characterization of the contributions of each medium, as demonstrated previously herein. In addition, the approaches previously presented in the literature decouple the

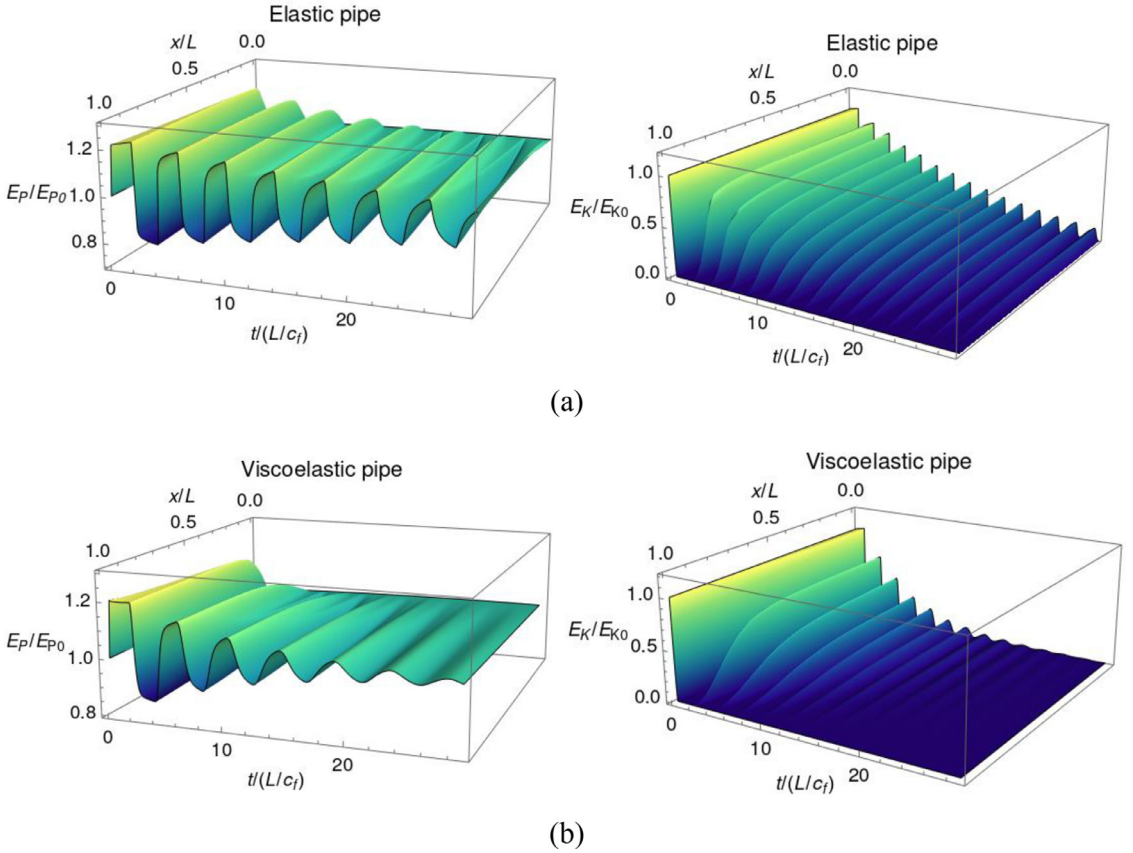

Fig. 11. Normalized pressure head and velocity head energies of the fluid for the experimental setup of Covas [53]. Comparison between the responses for (a) the elastic and (b) the viscoelastic tube.

pipe and fluid responses in the analysis as they do not have other means to view the effect of each medium in an isolated way. Such an approach rules out the mechanical interaction between the pipe wall and the fluid flow, which exists and which is put in evidence in what follows.

The overall rate of energy dissipation in both fluid and pipe through the pipe extension provides a broader view of how the energy dissipation takes place in the coupled fluid-pipe system. These overall rates can be defined as $D_k = \int_0^L d_k(x, t)dx$, where $k \in \{f, p\}$. Fig. 10 shows a comparison between the histories of the overall rate of energy dissipation through the pipe extension (normalized by $D_{f0} = \int_0^L d_f(x, 0)dx$), when the pipe exhibits elastic and viscoelastic mechanical responses. When compared to the elastic case, the viscoelastic case dissipates more energy in the first moments of the event. The reason is evident, the significant rates of energy dissipation that occur in the viscoelastic pipe. However, if one looks solely at the fluid dissipation in both cases, one may realize that the fluid dissipation in the elastic pipe case is always superior. In addition, in the elastic case, meaningful amounts of energy are dissipated until the late stages of the transient event, which does not occur when the pipe is viscoelastic. As the rate of energy dissipation in the fluid is proportional to the square of the fluid's velocity gradient in the radial direction for any pipe's mechanical response (see Eq. (32)), this result puts in evidence a two-way interaction between the fluid dynamics and pipe mechanical behavior.

The pressure fields for the elastic and viscoelastic pipes that have already been shown at a specific location in Fig. 4 can be broadly observed in the leftmost graphs of Figs. 11a and 11b, which present the local normalized pressure head energy, $E_P/E_{P0} = [p(x, t)/\rho_0 g]/[p(x,0)/\rho_0 g]$, in the whole time-space span. The amount of energy dissipated by the viscoelastic behavior of the pipe makes the pressure attenuation and dispersion more intense in the whole extension of the pipe. Such energy dissipation also induces the reduction of the levels of the normalized velocity head energy, $E_K/E_{K0} = [v^2/2]/[{v_0}^2/2]$, at superior rates than those found in the elastic pipe, as shown in the rightmost plots of Figs. 11a and 11b. Consequently, the decay of the cross-sectionally average velocity of the fluid v achieved by the viscoelastic pipe is more pronounced. As the initial averaged fluid velocity is the same for the elastic and viscoelastic cases, the loss of kinetic energy can also be related to the less pronounced velocity gradients in the fluid flow found in the viscoelastic case as shown in Fig. 12. As presented in Fig. (11), the fluid's kinetic energy is similar in the first moments of the transient for both pipe's material behavior. Nevertheless, as the pipe dissipates energy (Fig. 9), the fluid's kinematic responses attenuate, and the differences between the

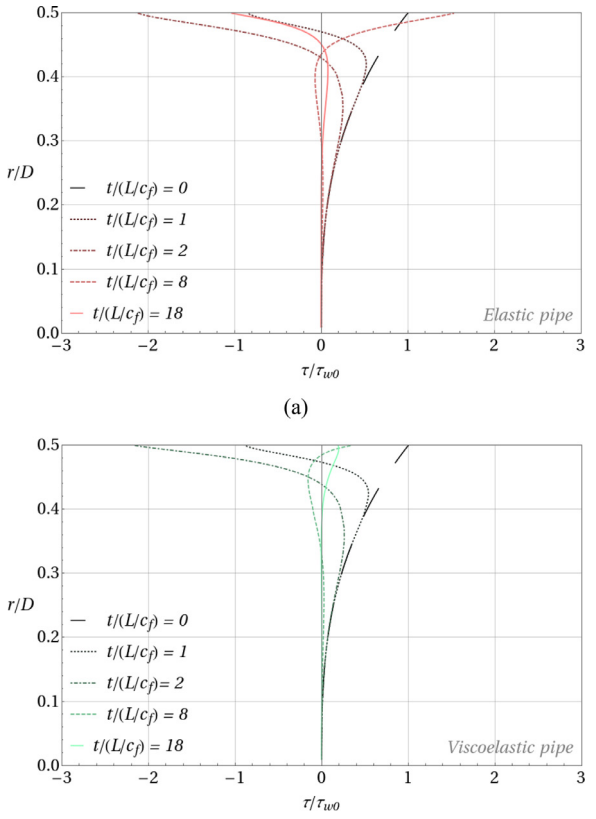

Fig. 12. Normalized shear-stress profiles at the mid-length of the pipe at different normalized times. Comparison between the responses of (a) the elastic and (b) the viscoelastic tube.

Table 5
Polyethylene (PE) pipe described in Urbanowicz et al. [21].

$\nu_0[-]$	$E_0[10^9 Pa]$	$E_1[10^9 Pa]$	$E_2[10^9 Pa]i$	$\tau_1[s]$	$\tau_2[s]$
0.38	0.45	0.48	0.28	0.0347	3.077

velocity profiles for the case of elastic and viscoelastic materials becomes discernible at later stages of the fluid transient (see Fig. 12).

The mechanical coupling between the fluid and the pipe is now explored in one more example. By replacing the HDPE pipe applied in the experiment of Covas [53] with the polyethylene pipe described in Table 5, one can note in Fig. 13 that not only the pipe's energy dissipation is influenced, but the energy dissipation in the fluid is also affected. In the pipe, more significant energy dissipation values are observed compared to the original case (see Fig. 9a). Moreover, the dissipation in the pipe is even more concentrated in the first cycle of the transient. The rate of energy dissipation in the fluid flow maintained a similar overall format, but the levels of dissipated energy are vastly reduced (see Fig. 9b).

Some insights into the reasons behind this behavior can be achieved. The larger period of oscillation (L/c_f) reduces the shear stress values in the fluid flow, which in turn causes less energy dissipation [60]. At the same time, the extended wave period and the less rigid Young 's moduli of the Kelvin-Voigt units in the PE pipe allow the pipe to dissipate a more significant amount of energy in the first cycle of the transient. In addition, the reduction of the transient intensity (measured by the product $\rho_0 c_f v_0$) also shrinks the responses of both pipe and fluid media. The amount of energy dissipated by the pipe, together with the minor fluid transient intensity turn the pressure head and velocity head energies to be less acute and more rapidly damped than when compared to the previous HDPE pipe (see Fig. 14).

The preceding paragraph grasps some reasons that lie behind the distinct responses for different viscoelastic pipes. However, all these effects mentioned above occur simultaneously, and the pipe and fluid mechanical reactions influence each other instantaneously, in such a way that taking into account this fluid-pipe interaction is required for an accurate description of the fluid transient. Further, the pipe and fluid flow behavior depend not only on geometrical properties but also on a

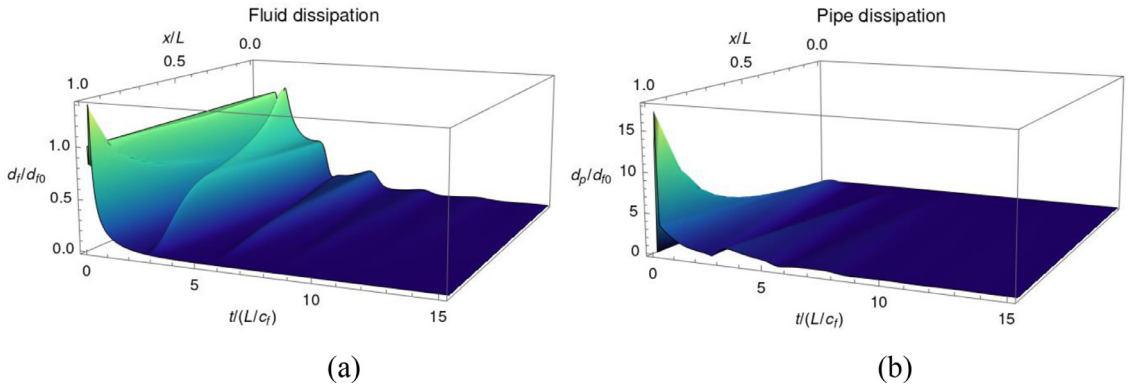

Fig. 13. Normalized local rate of energy dissipation in (a) the fluid and (b) the pipe for the setup of Covas [53] when the pipe is made of PE as described in Table 3.

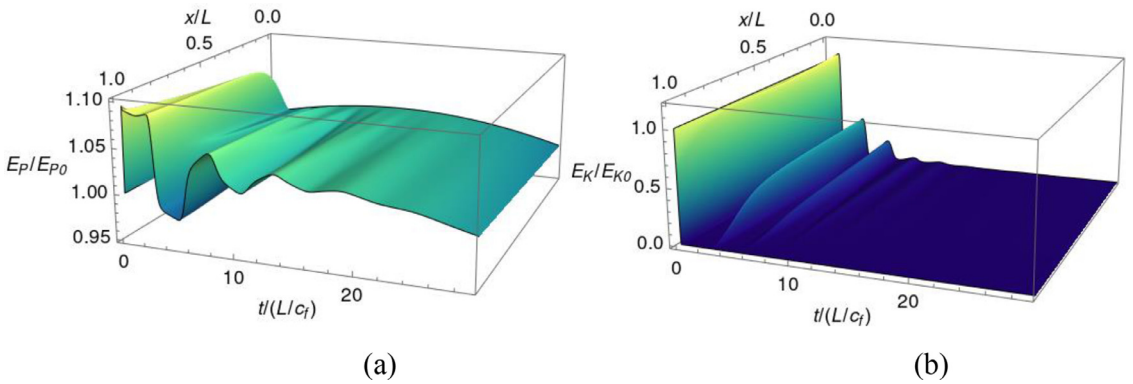

Fig. 14. Normalized (a) pressure head and (b) velocity head energies of the fluid for the experimental setup of Covas [53] when the pipe is made of PE as described in Table 3.

significant number of constitutive parameters (e.g., different relaxation times for the same viscoelastic pipe). A generalized study of the fluid transient responses for different flow conditions and viscoelastic constitutive constants can expose a better picture of the phenomenon. However, it is a demanding task that is out of the scope of the present work.

Nevertheless, the present analysis reveals that by ignoring the viscoelasticity of the pipe, the model overlooks crucial thermomechanical mechanisms of the coupled fluid-pipe system which can lead to poor results for the computed transient responses (e.g., Fig. 4). The results also show that accurate computation of the rate of energy dissipation in the fluid and pipe separately provides a reliable and powerful tool to discern the local and overall significance of the viscoelasticity and the transient fluid friction during the event. Such a result can be constructive to further theoretical and practical analysis in the field.

8. Summary and conclusions

This work presents a fluid transient model capable of handling the viscoelastic behavior of the pipe. A previously developed quasi-2D flow model is used as a base, and the viscoelastic characteristic of the pipe is included according to constitutive equations formulated in a thermodynamic consistent framework of an internal variable theory. Besides the model's capability to predict pressure-head histories with great accuracy, the model allows computing the rates of energy dissipation in the fluid and pipe distinctly and accurately. After validating the model against experimental results, the crucial role of the viscoelasticity of the pipe material in the transient responses is accessed by establishing a comparison with those observed in elastic pipe materials. The results show that in addition to delaying the pressure oscillations, the viscoelastic behavior brings a faster attenuation of the pressure loadings to which the pipe is subject. Even though such a result is already known, the present work takes advantage of its capacity to compute the rates of energy dissipation in the pipe and in the fluid to provide a better understanding of the underlying mechanisms. The energy dissipation in the pipe has superior magnitudes compared to those found in the fluid. Then, the system as a whole loses a significant part of its energy content, which is reflected as attenuated responses of the pressure and kinematic energies. The capability of computing the energy dissipation separately for fluid and pipe also exposes that each dissipative mechanism - although intensively tied -

is intrinsically different. It has also been shown that the alteration of the viscoelastic characteristics of the pipe affects the fluid hydrodynamics.

To conclude, this work puts in evidence that an accurate computation of the energy dissipation of the pipe and the fluid separately can be a direct and promising tool to better comprehend the fluid transient behavior in viscoelastic piping systems. Aside from the theoretical importance, the energy dissipation can be relevant to the development of equipment for damping the water hammer and life time prediction due to fatigue in plastic pipes [61–62].

Data availability

Data will be made available on request.

Acknowledgements

This study was financed by the Coordenação de Aperfeiçoamento de Pessoal de Nível Superior - Brasil (CAPES) - Finance Code 001 and by the Fundação Carlos Chagas Filho de Amparo à Pesquisa do Estado do Rio de Janeiro (FAPERJ). The first author also thanks the Eindhoven University of Technology for providing the needed structure to complete this work.

Appendix A. Procedure to achieve the expressions of the fluid's material constants

Under the assumptions of the model, the steady-state momentum balances for the $j-th$ constituents Eq. (6)) are sufficient for determining the material constants of the model. By employing the proposed expressions of the reactive force a_j and internal forces m_j, Eqs. (4-(5), in addition to the restriction $C_{j,j+1} = C_{j+1,j}$, this balance generates a linear system of equations whose solution are the material constants of the model, C and $C_{j,j+1}$, for $j = 1, \ldots, n$. Such a linear system may be solved by making use of known expressions of velocity profiles in steady-state. The foregoing approach is general for laminar or turbulent flows. By appealing to the velocity profiles found in laminar flows

$$v\left(R_j\right) = \frac{R^2}{4\rho_0 \nu}\left[1 - \left(\frac{R_j}{R}\right)^2\right]\left(-\frac{dp}{dx}\right), \tag{A.1}$$

the steady-state momentum balances for the constituents can be resumed to:

$$\begin{aligned}
&C_{1,2}\left[(R_2)^2 - (R_1)^2\right] = \phi\alpha_1,\\
&C_{2,1}\left[(R_1)^2 - (R_2)^2\right] + C_{2,3}\left[(R_3)^2 - (R_2)^2\right] = \phi\alpha_2,\\
&C_{j,j-1}\left[\left(R_{j-1}\right)^2 - \left(R_j\right)^2\right] + C_{j,j+1}\left[\left(R_{j+1}\right)^2 - \left(R_j\right)^2\right] = \phi\alpha_j,\\
&\vdots\\
&C_{n-1,n-2}\left[(R_{n-2})^2 - (R_{n-1})^2\right] + C_{n,n-1}\left[(R_n)^2 - (R_{n-1})^2\right] = \phi\alpha_{n-1},\\
&\frac{2}{R}C\left[R^2 - (R_n)^2\right] + C_{n,n-1}\left[(R_{n-1,\ n})^2 - (R_n)^2\right] = \phi\alpha_n,
\end{aligned} \tag{A.2}$$

in which, $\phi = 4\rho_0\nu$. As $C_{j,j+1} = C_{j+1,\ j}$, a recursive strategy starting from the first expression shown in Eq. (A.2) can be employed to find the solution to the system given by:

$$\begin{aligned}
&C_{j,\ j+1} = \frac{4\rho_0\nu}{R_{j+1}^2 - R_j^2}\left(\sum_{i=1}^{j}\alpha_i\right), \text{ with } R_{n+1} \equiv 0,\\
&C = \frac{2\ \rho_0\nu R}{R^2 - R_n^2}.
\end{aligned} \tag{A.3}$$

In turbulent flows, the steady-state balance for each constituent cannot be simplified as presented above. The dependence of the turbulent velocity profile on the logarithm of the radius of the $j-th$ constituent,

$$v\left(R_j\right) = \begin{cases}
\dfrac{\left(-\frac{dp}{dx}\right)}{\rho_0\nu_w}\left\{\dfrac{R_M^2 - \left(R_j\right)^2}{4(\sigma_{cw})} - \dfrac{b^2}{2}\left[\dfrac{-1}{(1-\sigma_{cw})} + \dfrac{(-4+5\sigma_{cw})}{(1-\sigma_{cw})^2}\ln\left(\dfrac{1}{\sigma_{cw}}\right)\right]\right\}, & 0 \le r \le R_M\\
\dfrac{\left(-\frac{dp}{dx}\right)b^2}{2\nu_w\ \rho_0}\left\{\dfrac{\left(R - R_j\right)}{(1-\sigma_{cw})b} + \dfrac{(4-5\sigma_{cw})}{(1-\sigma_{cw})^2}\ln\left[\dfrac{1}{\frac{(1-\sigma_{cw})}{b}\ R_j\ - 4 + 5\sigma_{cw}}\right]\right\}, & R_M < r \le R
\end{cases} \tag{A.4}$$

yields the steady-state balances of momentum for each constituent to be given as

$$\begin{aligned}
&C_{1,2}\Lambda_1 = \alpha_1,\\
&-C_{2,1}\Lambda_1 + C_{2,3}\Lambda_2 = \alpha_2,\\
&\vdots\\
&-C_{j,j-1}\Lambda_{j-1} + C_{j,j+1}\Lambda_j = \alpha_j,\\
&\vdots\\
&-C_{n-1,n-2}\Lambda_{n-2} + C_{n,n-1}\Lambda_{n-1} = \alpha_{n-1},\\
&-C_{n,n-1}\Lambda_{n-1} + \frac{2}{R}C\nu_n = \alpha_j,
\end{aligned} \tag{A.5}$$

where

$$\Lambda_j = \begin{cases} \dfrac{\left(R_{j+1}\right)^2 - \left(R_j\right)^2}{4\rho_0\nu_c}, & 0 \le R_j \le R_M \\ \dfrac{b^2}{2\nu_w\rho_0}\left[\dfrac{R_{j+1}-R_j}{(1-\sigma_{cw})b} + \dfrac{(-4+5\sigma_{cw})}{(1-\sigma_{cw})^2}\ln\left[\dfrac{\left(\frac{1-\sigma_{cw}}{b}\right)R_j - 4 + 5\sigma_{cw}}{\left(\frac{1-\sigma_{cw}}{b}\right)R_{j+1} - 4 + 5\sigma_{cw}}\right]\right], & R_M < R_j \le R \end{cases}. \tag{A.6}$$

The same recursive strategy applied for the laminar flow case can also be used to achieve the core, annular, and skin-friction material constants of the model:

$C_{j,j+1} = \frac{4\rho_0\nu_c}{R_{j+1}^2 - R_j^2}\left(\sum_{i=1}^{j}\alpha_i\right)$, for $0 \le R_j \le R_M$.

$$C_{j,j+1} = \frac{2\nu_w\rho_0(1-\sigma_{cw})/b^2}{\left\{\frac{R_{j+1}-R_j}{b} + \frac{(-4+5\sigma_{cw})}{(1-\sigma_{cw})}\ln\left[\frac{\left(\frac{1-\sigma_{cw}}{b}\right)R_j - 4 + 5\sigma_{cw}}{\left(\frac{1-\sigma_{cw}}{b}\right)R_{j+1} - 4 + 5\sigma_{cw}}\right]\right\}}\left(\sum_{i=1}^{j}\alpha_i\right), \text{ for } R_M < R_j \le R_{n-1},$$

$$C = \frac{\nu_w\rho_0 R(1-\sigma_{cw})/b^2}{\left\{\frac{R-R_n}{b} + \frac{(-4+5\sigma_{cw})}{(1-\sigma_{cw})}\ln\left[\left(\frac{1-\sigma_{cw}}{b}\right)R_n - 4 + 5\sigma_{cw}\right]\right\}}, \text{ for } R_j = R_n \tag{A.7}$$

Appendix B. The final form of the balance of mass

The state law given by Eq. (23) can be used to achieve the following stress-strain relation:

$$\varepsilon_\theta|_{r=R} = \frac{1}{E_0}[\sigma_\theta|_{r=R} - \nu_0\sigma_r|_{r=R}] - \frac{\nu_0}{E_0}\sigma_x|_{r=R} + \varepsilon_\theta^a|_{r=R}. \tag{B.1}$$

Thus, the balance of mass can be expressed as

$$\frac{1}{K}\frac{\partial p}{\partial t} + \frac{\partial v}{\partial x} + \frac{2}{R}\frac{\partial}{\partial t}\left[\frac{1}{E_0}(\sigma_\theta|_{r=R} - \nu_0\sigma_r|_{r=R}) - \frac{\nu_0}{E_0}\sigma_x|_{r=R} + \varepsilon_\theta^a|_{r=R}\right] = 0. \tag{B.2}$$

The values for the circumferential and radial stresses at the internal pipe wall obtained for a solid ring subject to internal pressure loadings establish that [50]:

$$\sigma_\theta|_{r=R} - \nu_0\sigma_r|_{r=R} = \left[\frac{R}{e} + \frac{\left(1+\frac{e}{R}\right)}{\left(2+\frac{e}{R}\right)} + \nu_0\right]p. \tag{B.3}$$

Moreover, one can assume that the variation of the axial stress in the pipe-wall's cross-section is small such that

$$\sigma_x|_{r=R} = \overline{\sigma_x} = \nu_0\left(\overline{\sigma_r} + \overline{\sigma_\theta}\right), \tag{B.4}$$

in which the superimposed bar symbol $\bar{\Xi}$ stands for the cross-sectional averaged value of Ξ. Finally, assuming that anelastic circumferential strain is supposed to obey the following relation

$$\frac{1}{R}\varepsilon_\theta^a|_{r=R} = \frac{\left(R+\frac{1}{2}e\right)}{R}\overline{\varepsilon_\theta^a}, \tag{B.5}$$

the balance of mass can be expressed as

$$\left[\frac{1}{K} + \frac{2}{E_0}\left\{\frac{R}{e} + \frac{\left(1+\frac{e}{R}\right)}{\left(2+\frac{e}{R}\right)} + \nu_0 - \nu_0^2\Gamma\right\}\right]\frac{\partial p}{\partial t} + \frac{2\left(R+\frac{1}{2}e\right)}{R}\frac{\partial\varepsilon_\theta^a}{\partial t} + \frac{\partial v}{\partial x} = 0. \tag{B.6}$$

For the sake of simplicity, the bar superscripts were removed to follow the notation contained in the core manuscript.

Appendix C. Method of Characteristics

The governing equations given by Eq. (27) can be transformed into a canonical form:

$$\mathbf{A}\frac{\partial \mathbf{U}}{\partial t}+\mathbf{B}\frac{\partial \mathbf{U}}{\partial x}+\mathbf{C}=0 \tag{C.1}$$

in which the column vectors $\mathbf{U}$ and $\mathbf{C}$, and the matrices $\mathbf{A}$ and $\mathbf{B}$, are given by

$$\mathbf{U}=\left[\mathbf{U}_e^T \vdots \mathbf{U}_a^T\right]; \tag{C.2}$$

$$\mathbf{C}=\left[\mathbf{C}_e^T \vdots \mathbf{C}_a^T\right]; \tag{C.3}$$

$$\mathbf{A}=\begin{bmatrix} \mathbf{E} & \vdots & \mathbf{Q} \\ \dots & \vdots & \dots \\ 0 & \vdots & \mathbf{I}_\zeta \end{bmatrix}; \tag{C.4}$$

$$\mathbf{B}=\begin{bmatrix} \mathbf{K} & \vdots & 0 \\ \dots & \vdots & \dots \\ \mathbf{Z} & \vdots & 0 \end{bmatrix}, \tag{C.5}$$

where $\mathbf{U}_e(x,t)=\mathbf{U}_e$: $[0,\ L]\mathrm{x}\,[0,\ T]\subset\mathbf{R}^2, \mathbf{U}_a$: $[0,\ L]\mathrm{x}\,[0,\ T]\subset\mathbf{R}^\zeta$, with $\zeta = n-1+1+m$, are vectors that stand for the classic variables of the transient flow problem and the additional variables added because of the inclusion of the pseudo-mixture model and the anelastic nature of the structure, respectively. They are:

$$\mathbf{U}_e^T=[p\ v], \tag{C.6}$$

$$\mathbf{U}_a^T=\left[v_2\dots v_n\ \varepsilon_\theta^a\ \varepsilon_\theta^1\ \dots \varepsilon_\theta^m\ \right]. \tag{C.7}$$

The vectors of the source term $\mathbf{C}$ namely, $\mathbf{C}_e \in \mathbf{R}^2$ and $\mathbf{C}_a \in \mathbf{R}^\zeta$ are given by

$$\mathbf{C}_e^T=\left[0\ \frac{2}{R\rho_0}\ a_n\ \right], \tag{C.8}$$

$$\mathbf{C}_a^T=\left[c^2\dots\ c^n\ g_\theta\ g_1\ \dots\ g_m\right], \tag{C.9}$$

in which

$$c^j=\frac{m_j+\frac{2}{R}a_j}{\rho_0\alpha_j}, \tag{C.10}$$

$\mathbf{I}_\zeta$ is the identity matrix of size $\zeta\times\zeta$, and the matrices $\mathbf{E}\ \&\ \mathbf{K}\in\mathbf{R}^2\mathrm{x}\,\mathbf{R}^2$, $\mathbf{Z}\in\mathbf{R}^{2+\zeta}\,\mathrm{x}\,\mathbf{R}^2$, $\mathbf{Q}\in\mathbf{R}^2\mathrm{x}\,\mathbf{R}^{2+\zeta}$ are expressed as:

$$\mathbf{E}=\begin{bmatrix} \frac{1}{\rho_0 c_f^2} & 0 \\ 0 & 1 \end{bmatrix},\ \mathbf{K}=\begin{bmatrix} 0 & 1 \\ \frac{1}{\rho_0} & 0 \end{bmatrix},\ \mathbf{Z}=\begin{bmatrix} \frac{1}{\rho_0} & 0 \\ \vdots & \vdots \\ \frac{1}{\rho_0} & 0 \\ 0 & 0 \\ \vdots & \vdots \\ 0 & 0 \end{bmatrix},\ \mathbf{Q}=\begin{bmatrix} 0 & \dots & 0 & 2\Pi & 0 & \dots & 0 \\ 0 & \dots & 0 & 0 & 0 & \dots & 0 \end{bmatrix}. \tag{C.11}$$

The left multiplication of Eq. (C.1) by $\mathbf{A}^{-1}$ transforms this system of partial differential equation into:

$$\frac{\partial \mathbf{U}}{\partial t} + \mathbf{H}\frac{\partial \mathbf{U}}{\partial x} + \mathbf{F} = 0, \tag{C.12}$$

where $\mathbf{H}$ and $\mathbf{F}$ are given by

$$\mathbf{H} = \mathbf{A}^{-1}\mathbf{B} = \begin{bmatrix} \mathbf{E}^{-1}\mathbf{K} & \vdots & 0 \\ \cdots & \vdots & \cdots \\ \mathbf{Z} & \vdots & 0 \end{bmatrix} = \begin{bmatrix} 0 & \rho_0 c_f^2 & \vdots & 0 \\ 1/\rho_0 & 0 & & \\ & \cdots & \vdots & \cdots \\ & \mathbf{Z} & \vdots & 0 \end{bmatrix}, \tag{C.13}$$

$$\mathbf{F} = \mathbf{A}^{-1}\mathbf{C} = \begin{bmatrix} \mathbf{E}^{-1}(\mathbf{C}_e - \mathbf{Q}\mathbf{C}_a) \\ \cdots \\ \mathbf{C}_a \end{bmatrix} = \begin{bmatrix} -2\Pi c_f^2 \rho_0 g_\theta \\ \dfrac{2}{R\rho_f}\, a_n \\ c_\nu^2 \\ \vdots \\ c_\nu^n \\ g_\theta \\ g_1 \\ \vdots \\ g_m \end{bmatrix}. \tag{C.14}$$

Equation (C.12) is classified as a quasi-linear system of partial differential equations and their characteristic curves are described by

$$\frac{dx}{dt} = \lambda_k, \tag{C.15}$$

in which λ_k are the eigenvalues associated with the matrix $\mathbf{H}$:

$$\det\left(\mathbf{H} - \lambda_k\, \mathbf{I}_{2+\zeta}\right) = 0. \tag{C.16}$$

This eigenvalue problem gives rise to the following characteristic polynomial:

$$\left(\lambda^2 - c_f^2\right)\lambda^\zeta = 0. \tag{C.17}$$

Thus, the following eigenvalues are found:

$$\begin{aligned} &\lambda_{1,2} = \pm c_f^2 \\ &\lambda_k = 0 \quad \text{for } k = 3, \ldots, \zeta. \end{aligned} \tag{C.18}$$

For each eigenvalue, left eigenvectors l_k are achieved by the following the relation

$$\begin{pmatrix} \cdots & l_k & \cdots \end{pmatrix}\left(\mathbf{H} - \lambda_k\, \mathbf{I}_{2+\zeta}\right) = 0, \tag{C.19}$$

which produces:

$$
\begin{aligned}
l_1 &= \left[\frac{1}{\rho_0 c_f}\ 1\ 0_{1,n-1+1+m}\right],\\
l_2 &= \left[-\frac{1}{\rho_0 c_f}\ 1\ 0_{1,n-1+1+m}\right],\\
l_3 &= [0\ -1\ 0\ 0\ 1\ 0_{1,n-2+1+m}],\\
l_4 &= [0\ -1\ 0\ 0\ 0\ 1\ 0_{1,n-3+1+m}],\\
l_5 &= [0\ -10\ 0\ 0\ 010_{1,n-4+1+m}],\\
&\vdots\\
l_{2+n-1} &= [0\ -1\ 0\ 0\ 0\ 0\ \ldots\ 0\ 1\ 0_{1,\,1+m}],\\
l_{2+1+n-1} &= [0\ -1\ 0\ 000\ \ldots\ 0\ 0\ 1\ 0_{1,\,m}],\\
l_{2+1+1+n-1} &= [0\ -1\ 0\ 0\ 0\ \ldots\ 0\ 10\ 0_{1,\,m-1}],\\
l_{2+2+1+n-1} &= [0\ -1\ 0\ 0\ 0\ \ldots\ 0\ 1\ 0\ 0\ 0_{1,\,m-2}],\\
&\vdots\\
l_{2+\zeta} &= [0\ -1\ 0\ 0\ 0\ \ldots\ 0\ 1].
\end{aligned}
\tag{C.20}
$$

These eigenvalues are all real and the eigenvectors form a set of linearly independent vectors. As a result, the set of partial differential equations given by Eq. (C.1) is classified as being merely hyperbolic. The method of characteristics (MOC) is an excellent method to solve such partial differential equations. The definition of the characteristic curve can be applied to express Eq. (C.12) as

$$
\mathbf{W}\left(\frac{d\mathbf{U}}{dt}+\mathbf{F}\right)=0, \tag{C.21}
$$

in which $\mathbf{W}=\begin{pmatrix}\cdots & l_1 & \cdots\\ \cdots & \vdots & \cdots\\ \cdots & l_{2+\zeta} & \cdots\end{pmatrix}$ is a square matrix composed by the left eigenvectors of the system. Hence, the system of partial differential equations can be expressed as

$$
\begin{aligned}
&\frac{1}{\rho_0\, c_f}\frac{dp}{dt}+\frac{dv}{dt}+\frac{2}{R\rho_0}\,a_n\ -\ 2c_f\Pi g_\theta=0 \quad \text{along } C_f^+ \ \equiv\ \frac{dx}{dt}=c_f\\
&-\frac{1}{\rho_0\, c_f}\frac{dp}{dt}+\frac{dv}{dt}+\frac{2}{R\rho_0}a_n+2c_f\Pi g_\theta=0 \quad \text{along } C_f^- \ \equiv\ \frac{dx}{dt}=-c_f,\\
&-\frac{dv}{dt}+\frac{dv_j}{dt}+\frac{m_j+\frac{2}{R}a_j}{\rho_0\alpha_j}-\frac{2}{R\rho_0}a_n\ =0,\quad j=2,\ \ldots n,\quad \text{along } C^0\equiv\ \frac{dx}{dt}=0\,,\\
&\frac{d\varepsilon_\theta^a}{dt}\ +\ g_\theta\ =\ 0\quad \text{along } C^0\equiv\ \frac{dx}{dt}=0,\\
&\frac{d\varepsilon_\theta^i}{dt}\ +\ g_i\ =0,\ i=1,\ldots,\ m\quad \text{along } C^0\equiv\ \frac{dx}{dt}=0.
\end{aligned}
\tag{C.22}
$$

References

[1] H. Ramos, D.I.C. Covas, A. Borga, D. Loureiro, Surge damping analysis in piping systems: modelling and experiments, J. Hydraul. Res. 42 (2004) 413–425, doi:10.1080/00221686.2004.9641209.

[2] A.K. Soares, D.I.C. Covas, L.F.R. Reis, Analysis of PVC pipe-wall viscoelasticity during water hammer, J. Hydaul. Eng. 134 (2008) 1389–1394, doi:10.1061/(ASCE)0733-9429(2008)134:9(1389).

[3] A. Triki, Comparative assessment of the inline and branching design strategies based on the compound technique, J. Water Supply 70 (2020) 155–170, doi:10.2166/aqua.2020.065.

[4] H.F. Brinson, L.C. Brinson, Polymer Engineering Science and Viscoelasticity: An Introduction, Springer, New York, 2008.

[5] E.B. Wylie, V.L. Streeter, Fluid Transients in Systems, Prentice Hall, Eaglewood Cliffs, New Jersey, 1993.
[6] E. Rieutord, A. Blanchard, Influence d'un comportement viscoélastique de la conduite dans le phénomène du coup de bélier (Influence of viscoelastic pipe behavior in the phenomenon of water hammer), Rep. Acad. Sci. 274 (1972) 1963–1966 274. (In French).
[7] P.G. Franke, F. Seyler, Computation of unsteady pipe flow with respect to viscoelastic material properties, J. Hydraul. Res. 21 (1983) 345–353, doi:10.1080/00221688309499456.
[8] M. Gally, M. Güney, E. Rieutord, An investigation of pressure transients in viscoelastic pipes, J. Fluid Eng. 101 (1979) 495–499, doi:10.1115/1.3449017.
[9] M.S. Güney, Waterhammer in viscoelastic pipes where cross-section parameters are time-dependent, in: Proc. 4th Int. Conf. Press. Surges, Pub. BHR Group, Bath, England, 1983, pp. 189–204.
[10] W. Zielke, Frequency-dependent friction in transient pipe flow, J. Basic Eng. 90 (1968) 109–115, doi:10.1115/1.3605049.
[11] D.I.C. Covas, I. Stoianov, H. Ramos, N. Graham, C. Maksimovic, D. Butler, Water hammer in pressurized pipes: conceptual model and experimental analysis, Urban Water J. 1 (2004) 177–197, doi:10.1080/15730620412331289977.
[12] H.F. Duan, M. Ghidaoui, P.J. Lee, Y.K. Tung, Unsteady friction and visco-elasticity in pipe fluid transients, J. Hydraul. Res. 48 (2010) 354–362, doi:10.1080/00221681003726247.
[13] F.B. Freitas Rachid, Clausius—Duhem inequality for quasi-1D transient flows in variables cross-section area deformable pipes, Appl. Math. Model. 100 (2021) 491–507, doi:10.1016/j.apm.2021.07.040.
[14] G. Pezzinga, B. Brunone, D. Cannizzaro, M. Ferrante, S. Meniconi, A. Berni, Two-dimensional features of viscoelastic models of pipe transients, J. Hydraul. Eng. 140 (2014) 1–9, doi:10.1061/(ASCE)HY.1943-7900.0000891.
[15] E.M. Wahba, On the two-dimensional characteristics of laminar fluid transients in viscoelastic pipes, J. Fluids Struct. 68 (2017) 113–124, doi:10.1016/j.jfluidstructs.2016.10.012.
[16] S. Meniconi, B. Brunone, M. Ferrante, Water-hammer pressure waves interaction at cross-section changes in series in viscoelastic pipes, J. Fluids Struct. 33 (2012) 44–58, doi:10.1016/j.jfluidstructs.2012.05.007.
[17] M. Kubrak, A. Malesinska, A. Kodura, K. Urbanowicz, M. Stosiak, Hydraulic transients in viscoelastic pipeline system with sudden cross-section changes, Energies 14 (2021) 4071, doi:10.3390/en14144071.
[18] S. Vlase, M. Marin, M.L. Scutaru, D.D. Scărlătescu, C. Csatlos, Study on the mechanical responses of plastic pipes made of high density polyethylene (HDPE) in water supply network, Appl. Sci. 10 (2020) 1–22, doi:10.3390/app10051658.
[19] P. Chahardah-Cherika, M. Fathi-Moghadama, S. Haghighipoura, Modelling of transient flows in viscoelastic pipe network with partial blockage, J. Water Supply 70 (2021) 832–844, doi:10.2166/aqua.2021.040.
[20] A.K. Soares, D.I.C. Covas, N.J.G. Carriço, Transient vaporous cavitation in viscoelastic pipes, J. Hydraul. Res. 50 (2012) 228–235, doi:10.1080/00221686.2012.669143.
[21] K. Urbanowicz, A. Bergant, A. Kodura, M. Kubrak, A. Malesinska, P. Bury, M. Stosiak, Modeling transient pipe flow in plastic pipes with modified discrete bubble cavitation model, Energies 14 (2021) 6756, doi:10.3390/en14206756.
[22] M. Mousavifard, Turbulence parameters during transient cavitation flow in viscoelastic pipe, J. Hydraul. Eng. 148 (2022) 04022004, doi:10.1061/(ASCE)HY.1943-7900.0001973.
[23] T.G. Che, H.F. Duan, P.J. Lee, Transient wave-based methods for anomaly detection in fluid pipes: a review, Mech. Syst. Signal Process. 160 (2021) 107874, doi:10.1016/j.ymssp.2021.107874.
[24] H.F. Duan, S. Meniconi, P.J. Lee, B. Brunone, M.S. Ghidaoui, Local and integral energy-based evaluation for the unsteady friction relevance in transient pipe flows, J. Hydraul. Eng. 143 (2017) 1–11, doi:10.1061/(ASCE)HY.1943-7900.0001304.
[25] G. Pezzinga, P. Scandura, Unsteady flow in installations with polymeric additional pipe, J. Hydraul. Eng. 121 (1995) 802–811, doi:10.1061/(ASCE)0733-9429(1995)121:11(802).
[26] A.S. Tijsseling, A.E. Vardy, On the suppression of coupled liquid/pipe vibrations, in: Proc. 18th IAHR Symp. on Hydraulic Machinery and Cavitation, Kluwer Academic Publishers, 1996 (Editors E. Cabrera, V. Espert, F. Martínez), Valencia, Spain945-954; Dordrecht, The NetherlandsISBN 0-7923-4210-0.
[27] G. Pezzinga, Unsteady flow in hydraulic networks with polymeric additional pipe, J. Hydraul. Eng. 128 (2002) 238–244, doi:10.1061/(ASCE)0733-9429(2002)128:2(238).
[28] A. Triki, Water-hammer control in pressurized-pipe flow using an in-line polymeric short-section, Acta Mech. 227 (2016) 777–793, doi:10.1007/s00707-015-1493-1.
[29] A. Triki, Further investigation on water-hammer control inline strategy in water-supply systems, J. Water Supply 67 (2018) 30–43, doi:10.2166/aqua.2017.073.
[30] J. Gong, M. Stephens, M.F. Lambert, A.C. Zecchin, A.R. Simpson, Pressure surge suppression using a metallic-plastic-metallic pipe configuration, J. Hydraul. Eng. 144 (2018) 04018025, doi:10.1061/(ASCE)HY.1943-7900.0001468.
[31] R.B. Iffa, A. Triki, Assessment of inline technique-based water hammer control strategy in water supply systems, J. Water Supply 68 (2019) 562–572, doi:10.2166/aqua.2019.095.
[32] M. Kubrak, A. Malesińska, A. Kodura, K. Urbanowicz, P. Bury, M. Stosiak, Water hammer control using additional branched HDPE pipe, Energies 14 (2021) 8008, doi:10.3390/en14238008.
[33] B.W. Karney, Energy relations in transient closed-conduit flow, J. Hydraul. Eng. 116 (1990) 1180–1196, doi:10.1061/(ASCE)0733-9429(1990)116:10(1180).
[34] B. Pan, A. Keramat, C. Capponi, S. Meniconi, B. Brunone, H.F. Duan, Transient energy analysis in water-filled viscoelastic pipelines, J. Hydraul. Eng. 1 (2021) (2021) 04021051, doi:10.1061/(ASCE)HY.1943-7900.0001959.
[35] J. Lemaitre, J.L. Chaboche, Mechanics of Solid Materials, Cambridge University Press, New York, 1990.
[36] G.A. Mauguin, The Thermomechanics of Nonlinear Irreversible Behaviors, World Scientific Publishing Co, Singapore, 1999.
[37] D.M. Andrade, F.B. Freitas Rachid, A versatile friction model for Newtonian liquids flowing under unsteady regimes in pipes, Meccanica 57 (2022) 43–72, doi:10.1007/s11012-021-01458-5.
[38] R.J. Atkin, R.E. Craine, Continuum theories of mixtures: basic theory and historical development, Q. J. Mech. Appl. Math. 29 (1976) 209–244, doi:10.1093/qjmam/29.2.209.
[39] A.E. Vardy, J.M.B. Brown, S. He, C. Ariyaratne, S. Gorji, Applicability of frozen-viscosity models of unsteady wall shear stress, J. Hydraul. Eng. 141 (2015) 04014064, doi:10.1061/(ASCE)HY.1943-7900.0000930.
[40] A.E. Vardy, J.M.B. Brown, Approximation of turbulent wall shear stresses in highly transient pipe flows, J. Hydraul. Eng. 133 (2007) 1219–1228, doi:10.1061/(ASCE)0733-9429(2007)133:11(1219).
[41] M.E. Gurtin, F. Eliot, L. Anand, The Mechanics and Thermodynamics of Continua, Cambridge University Press, New York, 2009.
[42] G.A. Maugin, W. Muschik, Thermodynamics with internal variables: Part I, J. Non-equil. Thermody. 19 (1994) 217–289, doi:10.1515/jnet.1994.19.3.217.
[43] F.B. Freitas Rachid, H.S. Costa Mattos, S. Stuckenbruck, Waterhammer in Inelastic Pipes: an approach via internal variable constitutive Theory, in: Proc. Inter. Conf. on Unsteady Flow and Fluid Transients, Balkema, Rotterdam, The Netherlands, 1992 63-70. ISBN 90 5410 046 X.
[44] A. Keramat, A. Gaffarian Kolahi, A. Ahmadi, Waterhammer modelling of viscoelastic pipes with a time-dependent Poisson's ratio, J. Fluids Struct. 43 (2013) 164–178, doi:10.1016/j.jfluidstructs.2013.08.013.
[45] A. Keramat, K. Heidari Shirazi, Finite element based dynamic analysis of viscoelastic solids using the approximation of Volterra integrals, Finite Elem. Anal. Des. 86 (2014) 89–100, doi:10.1016/j.finel.2014.03.010.
[46] K. Weinerowska-Bords, Viscoelastic model of waterhammer in single pipeline—problems and questions, Arch. Hydro. Eng. Environ. Mech. 53 (2006) 331–351.
[47] K. Weinerowska-Bords, Accuracy and parameter estimation of elastic and viscoelastic models of the water hammer, Task Q 11 (2007) 383–395.
[48] D.I.C. Covas, I. Stoianov, J. Mano, H. Ramos, N. Graham, C. Maksimovic, The dynamic effect of pipe-wall viscoelasticity in hydraulic transients. Part I - experimental analysis and creep characterization, J. Hydraul. Res. 42 (2004) 516–530, doi:10.1080/00221686.2004.9641221.

[49] D.I.C. Covas, I. Stoianov, J. Mano, H. Ramos, N. Graham, C. Maksimovic, The dynamic effect of pipe-wall viscoelasticity in hydraulic transients. Part II - model development, calibration and verification, J. Hydraul. Res. 43 (2005) 56–70, doi:10.1080/15730620412331289977.
[50] A.S. Tijsseling, Water-hammer with fluid-structure interaction in thick-walled pipes, Comput. Struct. 85 (2007) 844–851, doi:10.1016/j.compstruc.2007.01.008.
[51] H.S. Costa Mattos, M.L. Martins-Costa, R.M. Saldanha da Gama, On the modeling of momentum and energy transfer in incompressible mixtures, Int J. Non Linear Mech. 30 (1995) 419–431, doi:10.1016/0020-7462(95)00016-H.
[52] R.T. Rockafellar, Convex Analysis, Princeton University Press, Princeton, 1970.
[53] D.I.C. Covas, Inverse Transient Analysis for Leak Detection and Calibration of Water Pipe Systems - Modelling Special Dynamic Effects. PhD Thesis, Imperial College of Science, Technology and Medicine, University of London, London, UK.
[54] K. Urbanowicz, H.F. Duan, A. Bergant, Transient liquid flow in plastic pipes, J. Mech. Eng 66 (2020) 77–90, doi:10.5545/sv-jme.2019.6324.
[55] K. Urbanowicz, A. Bergant, H.F. Duan, U. Karadzić, D. Sobków, Alternative numerical solution of transient flow in viscoelastic pipes, J. Phys. Conf. Series 1736 (2021) 012038, doi:10.1088/1742-6596/1736/1/012038.
[56] H.A.A. Abdel-Gawad, B. Djebdjian, Modelling water hammer in viscoelastic pipes using the wave characteristic method, Appl. Math. Model. 83 (2020) 322–341, doi:10.1016/j.apm.2020.01.045.
[57] S. Saeml, M. Raisee, M. Cervantes, A. Nourbakhsh, Computation of two and three-dimensional water hammer flows, J. Hydraul. Res. 57 (2019) 386–404, doi:10.1080/00221686.2018.1459892.
[58] D.M. Andrade, F.B. Freitas Rachid, A.S. Tijsseling, A new model for fluid transients in piping systems taking into account the fluid-structure interaction, J. Fluids Struct. 104 (2022) 103720, doi:10.1016/j.jfluidstructs.2022.103720.
[59] A. Seck, Numerical solutions of hyperbolic systems of conservation laws combining unsteady friction and viscoelastic pipes, J. Hydroinform. 23 (2021) 103–116, doi:10.2166/hydro.2020.119.
[60] E.M. Wahba, A computational study of viscous dissipation and entropy generation in unsteady pipe flow, Acta Mech. 216 (2011) 75–86, doi:10.1007/s00707-010-0358-x.
[61] S. Folkman, R. Bishop, A simple design procedure for PVC pipe to account for cyclic pressure loading, in: Proc. 18th Plastic Pipes Conference, PPXVIII, Berlin, Germany, September, 2016, pp. 12–14.
[62] AWWAANSI/AWWA C900-16, Polyvinyl Chloride (PVC) Pressure Pipe and Fabricated Fittings, 4. in. through 60 in. (100 mm through 1,500 mm), American Water Works Association, 6666 W. Quincy Ave., Denver, CO 80235, USA, 2018.